



Ocean dynamic processes causing spatially heterogeneous distribution of sedimentary caesium-137 massively released from the Fukushima Daiichi Nuclear Power Plant

H. Higashi, Y. Morino, N. Furuichi, and T. Ohara

Center for Regional Environmental Research, National Institute for Environmental Studies, Tsukuba, Japan

Correspondence to: H. Higashi (higashi@nies.go.jp)

Received: 8 June 2015 – Published in Biogeosciences Discuss.: 11 August 2015

Revised: 2 November 2015 – Accepted: 18 November 2015 – Published: 8 December 2015

Abstract. Massive amounts of anthropogenic radiocaesium ^{137}Cs that were released into the environment by the Fukushima Daiichi Nuclear Power Plant accident in March 2011 are widely known to have extensively migrated to Pacific Ocean sediment off of eastern Japan. Several recent reports have stated that the sedimentary ^{137}Cs is now stable with a remarkably heterogeneous distribution. The present study elucidates ocean dynamic processes causing this heterogeneous sedimentary ^{137}Cs distribution in and around the shelf off Fukushima and adjacent prefectures. We performed a numerical simulation of oceanic ^{137}Cs behaviour for about 10 months after the accident, using a comprehensive dynamic model involving advection–diffusion transport in seawater, adsorption and desorption to and from particulate matter, sedimentation and suspension on and from the bottom, and vertical diffusion transport in the sediment. A notable simulated result was that the sedimentary ^{137}Cs significantly accumulated in a swath just offshore of the shelf break (along the 50–100 m isobath) as in recent observations, although the seabed in the entire simulation domain was assumed to have ideal properties such as identical bulk density, uniform porosity, and aggregation of particles with a single grain diameter. This result indicated that the heterogeneous sedimentary ^{137}Cs distribution was not necessarily a result of the spatial distribution of ^{137}Cs sediment adsorptivity. The present simulation suggests that the shape of the swath is mainly associated with spatiotemporal variation between bottom shear stress in the shallow shelf (<50 m depths) and that offshore of the shelf break. In a large part of the shallow shelf, the simulation indicated that strong bottom friction suspending

particulate matter from the seabed frequently occurred via a periodic spring tide about every 2 weeks and via occasional strong wind. The sedimentary ^{137}Cs thereby could hardly stay on the surface of the seabed with the result that the simulated sediment-surface ^{137}Cs activity tended to decrease steadily for a long term after the initial ^{137}Cs migration. By contrast, in the offshore region, neither the spring tide nor the strong wind caused bottom disturbance. Hence, the particulate matter incorporated with ^{137}Cs , which was horizontally transported from the adjacent shallow shelf, readily settled and remained on the surface of the sediment just offshore of the shelf break.

1 Introduction

In March 2011, the Great East Japan Earthquake (moment magnitude M_w 9.0) and subsequent huge tsunami caused a severe accident at the Fukushima Daiichi Nuclear Power Plant (1FNPP) operated by the Tokyo Electric Power Company (TEPCO). Massive anthropogenic radionuclides were thereby released from 1FNPP and extensively polluted the Pacific oceanic environment off of east Japan. The radiocaesium ^{137}Cs , one of the massively released radionuclides, was observed to reach a maximum $O(10^5)\text{ Bq L}^{-1}$ (we represent on the order of 10^n as $O(10^n)$) on the sea surface near 1FNPP just after the accident (early April 2011) (TEPCO, 2011). However, the seawater ^{137}Cs rapidly decreased down to less than $O(10^2)\text{ Bq L}^{-1}$ within a few months after the accident and finally $O(10^{-1})\text{ Bq L}^{-1}$ as of the end of 2011

(TEPCO, 2011; MEXT, 2011; Buesseler et al., 2011, 2012). By contrast, the sedimentary ^{137}Cs has been continuously detected with high activity ($> O(10^2)$ Bq kg $^{-1}$) in many sediment samples in the nearshore region off Fukushima and adjacent prefectures up to the present (e.g. Kusakabe et al., 2013; Thornton et al., 2013; Ambe et al., 2014; NRA, 2014a, b). There is no doubt that the ^{137}Cs remaining in the sediment is that which has migrated from the seawater to seabed. The total ^{137}Cs migration amount has been estimated as $O(10^{13}\text{--}10^{14})$ Bq (Kusakabe et al., 2013; Ambe et al., 2014; Otosaka and Kato, 2014). Because ^{137}Cs has a very long half-life (30.2 years), we should fully understand the long-term oceanic behaviour of the massive sedimentary ^{137}Cs to predict its fate and future impact on the marine environment and ecosystem.

Recent measurements have made it clear that variation in the sedimentary ^{137}Cs is spatially heterogeneous and temporally slow. Thornton et al. (2013) made in situ measurements of continuous ^{137}Cs distributions on the seabed surface between November 2012 and February 2013 using a towed gamma-ray spectrometer. Their results revealed the following non-uniform sedimentary ^{137}Cs distribution. High ^{137}Cs activities ($O(10^2\text{--}10^3)$ Bq kg $^{-1}$) on the sediment surface were detected in the nearshore region off 1FNPP (about 1–2 km east of the shore of 1FNPP) and offshore (beyond ~ 12 km east of the shore), but low concentrations ($O(10^1)$ Bq kg $^{-1}$) were detected between those regions. Ambe et al. (2014) collected samples with high spatial resolution (5' latitude and longitude) in the nearshore region south of Fukushima in February and July 2012. They found a high-activity region in the shape of a swath with width ~ 20 km along ~ 100 m isobath (we call this region the “hotspot swath” hereinafter). Considering also more recent published and unpublished measurements (e.g. NRA, 2014a), the hotspot swath possibly extended along the shelf edge (50–100 m depths) from the coastal region off of southern Fukushima to northeastern Sendai Bay off of Miyagi Prefecture. These features of the sedimentary ^{137}Cs distribution could not be captured by sediment sampling with poor spatial resolution (e.g. MEXT, 2011; TEPCO, 2011; Kusakabe et al., 2013).

The seabed in the hotspot swath mainly consists of fine particulate matter such as silt and clay (Thornton et al., 2013; Ambe et al., 2014; NRA, 2014a). Caesium is widely known to be readily and almost irreversibly adsorbed on the surface of fine-grained particles. It is thereby understood that sediment in the swath readily accumulated the oceanic ^{137}Cs . In fact, many observational studies have reported that the sedimentary ^{137}Cs distribution is correlated with sediment properties, especially particle grain size (e.g. Otosaka and Kobayashi, 2013; Kusakabe et al., 2013; Otosaka and Kato, 2014). However, there have been few studies on accumulation mechanisms of the fine particulate matter and sedimentary ^{137}Cs in the hotspot swath. The future fate of sedimentary ^{137}Cs in this swath has not been predicted or discussed.

Our primary objective was to elucidate ocean dynamic processes causing the spatially heterogeneous sedimentary ^{137}Cs distribution, especially in the hotspot swath. The study was based on numerical simulation of oceanic ^{137}Cs behaviour in and around the shelf off Fukushima and adjacent prefectures during March and December 2011.

To achieve our objective, a numerical model of oceanic ^{137}Cs behaviour requires with the treatment of comprehensive dynamic processes such as advection–diffusion in seawater, adsorption and desorption on and from the particulate matter, and sedimentation and suspension to and from the seabed (e.g. Perri  nez, 2003a, b, 2004, 2008; Kobayashi et al., 2007; Monte et al., 2009). Other numerical studies (Perri  nez et al., 2012; Choi et al., 2013) simulated spatiotemporal variation in sedimentary ^{137}Cs after the 1FNPP accident using such comprehensive models. However, they did not discuss the hotspot swath. This may be because their simulations were limited to only the 4 months after the accident, probably because of insufficient observations. Misumi et al. (2014) developed a simulation model of ^{137}Cs transfer between bottom seawater and the seabed, focusing on sediment adsorptivity with caesium evaluated from sediment properties such as particle grain diameter, bulk density, and porosity. They thereby succeeded in reproducing major features of the observed heterogeneous distribution of sedimentary ^{137}Cs during the first year after the 1FNPP accident. However, their simulation treated only ^{137}Cs activity on the surface of the sediment, using bottom-seawater ^{137}Cs simulated by another model in advance (offline simulation, unlike the aforementioned two studies). In addition, the spatial distribution of sediment adsorptivity with ^{137}Cs as input data was used by the model. Hence, accumulation mechanisms of either the fine particulate matter or sedimentary ^{137}Cs in the hotspot swath could not be depicted by their simulations.

There is another issue to be addressed by the aforementioned earlier models. They did not take into account the vertical ^{137}Cs distribution in the sediment, i.e. model variable sedimentary ^{137}Cs was given in only one active layer of the seabed surface. The studies regarded the layer of sediment incorporated with ^{137}Cs as sufficiently thin (within a few centimetres). However, it has been reported that the vertical sedimentary ^{137}Cs distribution was not necessarily uniform and that there were sites where sedimentary ^{137}Cs activity in deeper sediment (> 10 cm) was higher than that in upper sediment (Otosaka and Kobayashi, 2013; Ambe et al., 2014; NRA, 2014a). These observations suggest that the vertical ^{137}Cs profile in the sediment should be considered in modelling sedimentation and suspension processes. For instance, suspension of the sediment (incorporating ^{137}Cs) occurs successively from its upper portions. Although numerical models of only sediment transport have been developed with consideration of the vertical profiles of sediment properties in the seabed (e.g. Reed et al., 1999; Lesser et al., 2004; Blaas et al., 2007), there have been few models for vertical movement of other substances intricately connected with those properties.

There is also a severe problem in that data on the sediment property spatial distribution immediately after the 1FNPP accident, necessary for such simulation, are extremely limited because of the huge tsunami.

Our previous study (Higashi et al., 2014) developed a comprehensive model for simulating oceanic ^{137}Cs behaviour in both seawater and seabed, with consideration of vertical ^{137}Cs transport in the sediment. We then roughly assumed that sediment matter in the entire simulation domain had ideal properties such as identical bulk density, uniform porosity, and particle aggregates of a single grain diameter. The reason why we used this assumption was not only because spatiotemporal variation of sediment properties just after the tsunami disturbance was unknown but also because the assumption enabled direct simulation of vertical ^{137}Cs behaviour in the sediment. This type of assumption has also been used in other models (Kobayashi et al., 2007; Choi et al., 2013), except for the ^{137}Cs behaviour in sediment. Our earlier simulations using the developed model agreed reasonably well with the sampling of ^{137}Cs activity in both seawater and sediment off eastern Japan in the Pacific during March and December 2011. However, we could not effectively simulate the heterogeneous sedimentary ^{137}Cs distribution mainly because of a lack of spatial resolution.

We performed a downscaling simulation of oceanic ^{137}Cs behaviour using the usual one-way nesting method to resolve the heterogeneous sedimentary ^{137}Cs distribution, especially in the hotspot swath. The present simulation also used the aforementioned assumption of ideal sediment properties in the entire domain, for the same reasons. The model and the numerical procedure are described in Sect. 2. Simulated results of the spatiotemporal ^{137}Cs distributions in seawater and sediment within the nested region are shown in Sect. 3 as compared with observations to evaluate model performance. In Sect. 4, we discuss ocean dynamic processes causing the spatially heterogeneous distribution, especially in the hotspot swath, and include model uncertainties.

2 Model description

2.1 Outline

The numerical model in the present study was online-coupled with a hydrodynamic model (Sect. 2.2) and an oceanic ^{137}Cs behaviour model of seawater (Sect. 2.3) and sediment (Sect. 2.4) (Higashi et al., 2014). The function of the hydrodynamic model was to simulate three-dimensional oceanic currents, temperature, salinity, pressure, and others. The oceanic ^{137}Cs behaviour models of seawater and sediment dealt with spatiotemporal variations in concentrations of ^{137}Cs and particulate matter capable of adsorbing the ^{137}Cs . ^{137}Cs in our model was classified into two phases: dissolved ^{137}Cs and particulate ^{137}Cs , which was defined as ^{137}Cs adsorbing on the particulate matter. The oceanic

^{137}Cs behaviour model of seawater (hereinafter, “the seawater ^{137}Cs model”) was used to simulate ^{137}Cs advection-diffusion under ocean current conditions evaluated by the hydrodynamic model and simultaneous ^{137}Cs reactions such as adsorption/desorption on/from suspended particulate matter, settling, and radioactive decay (Fig. 1a). The oceanic ^{137}Cs behaviour model of the sediment (hereinafter, “the sediment ^{137}Cs model”) simulated sedimentation/suspension of ^{137}Cs and particulate matter between bottom seawater and surface sediment and subsequent changes in the vertical ^{137}Cs distribution in the seabed (Fig. 1). To connect the seawater and sediment ^{137}Cs models through sedimentation/suspension at the bottom interface, we used the aforementioned assumption of ideal sediment (i.e. particle aggregates with a single grain diameter, identical density, and uniform porosity), whose properties were equivalent to silty clay over the entire simulation domain. In the model, ^{137}Cs migrates from seawater to sediment through the following sequential processes: suspension of particulate matter from the seabed caused by erosion, vertical mixing of both suspended particulate matter and dissolved ^{137}Cs , formation of particulate ^{137}Cs through adsorption of dissolved ^{137}Cs on the suspended particulate matter, and sedimentation of the particulate ^{137}Cs on the bottom (Fig. 1a).

We carried out a regional-scale simulation of oceanic behaviour of the ^{137}Cs released from 1FNPP during March and December 2011. To simulate the heterogeneous sedimentary ^{137}Cs distribution in and around the shelf off Fukushima and adjacent prefectures, a high-spatial-resolution analysis was needed. In addition, because our target area is within the Kuroshio–Oyashio Interfrontal Zone (Yasuda et al., 1996) where there are strong currents and mesoscale eddy circulations, the model domain had to be sufficiently wide to simulate these essential dynamics. We therefore used a one-way nesting method for downscale simulation from a large area of the northwestern Pacific (Region-1) to a fine-resolution area (Region-2) (Fig. 2a). Region-1 covered 138.0–148.0° E and 32.0–41.0° N with horizontal resolutions of 4.5 km in longitude and 4.4 km in latitude. Region-2 covered 140.4–144.0° E and 35.2–39.0° N with horizontal resolutions 1.5 km in both longitude and latitude. Vertical layers in both regions were set to 47 levels in the seawater, from the sea surface to 6000 m depth, with thickness between 2 m (near the sea surface) and 500 m (near 6000 m depth). There were 42 levels in the sediment from the seabed surface to 1 m depth, with thickness from 0.01 m (near the seabed surface) to 0.05 m (near 1 m depth). Bathymetry was obtained by spatially interpolating gridded water-depth data of JTOPO30, provided by the Marine Information Research Center (MIRC), Japan Hydrographic Association.

2.2 Hydrodynamic model

The hydrodynamic model was originally developed and applied to several fields in our previous studies (e.g. Higashi

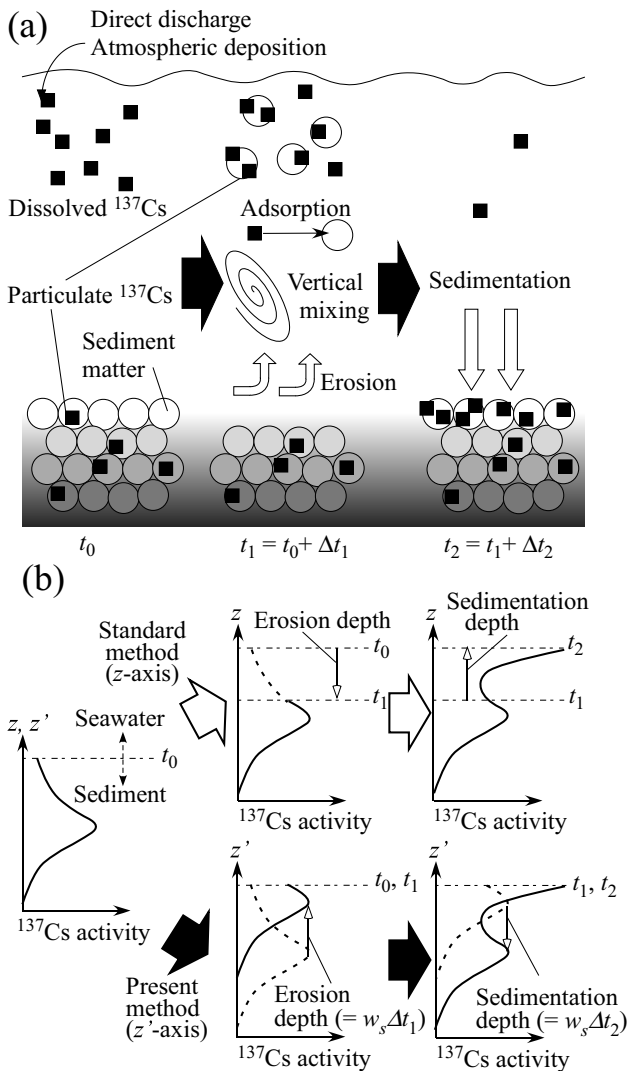


Figure 1. Schematic views of (a) processes of ^{137}Cs migration from seawater to sediment and (b) numerical procedure of vertical ^{137}Cs transport in sediment using z' coordinate defined in Sect. 2.4.

et al., 2011, 2013). This model was based on the three-dimensional hydrostatic Boussinesq equations, solved by the finite difference method using a horizontal collocated and vertical z -level grid (e.g. Ushijima et al., 2002). A free seawater surface as a vertical moving boundary was traced by the volume-of-fluid (VOF) method (Hirt and Nichols, 1981). Vertical mixing was evaluated using the latest turbulence-closure scheme (Furuichi et al., 2012; Furuichi and Hibiya, 2015), which was an improved version of the Nakanishi and Niino (2009) scheme. Horizontal eddy diffusion was calculated by the Smagorinsky (1963) formula.

Momentum and heat exchanges between ocean and atmosphere, which were the seawater surface boundary conditions, were evaluated using the Kondo (1975) method. For these evaluations, we used the following meteorologi-

cal data at/above the sea surface: hourly atmospheric pressure, wind velocity, air temperature, specific humidity, and precipitation from the Grid Point Value of Mesoscale Model (GPV/MSM) of the Japan Meteorological Agency (JMA). Six-hourly downward solar and long-wave radiation data were from the JMA Climate Data Assimilation System (JC-DAS).

In the Region-1 simulation, we specified daily-mean data of salinity and temperature at the lateral boundaries, reanalysed by FRA-JCOPE2 (the Japan Coastal Ocean Predictability Experiment 2 developed by Japan Agency for Marine-Earth Science and Technology in collaboration with Fisheries Research Agency) (Miyazawa et al., 2009). The FRA-JCOPE2 data were also used for simple three-dimensional nudging of salinity and temperature to involve observed/assimilated features of geostrophic phenomena in our simulation. Reference data for the nudging were 10-day moving average time series of the FRA-JCOPE2 results. A parameter of nudging timescale was set to 20 days. The Region-2 simulation used the same methods for the lateral boundaries and nudging of temperature and salinity as in the Region-1 simulation, but the hourly Region-1 simulations provided the input data instead of FRA-JCOPE2.

Sea-surface elevation at the open boundaries in the Region-1 simulation was from a composite of mean level and tidal anomaly. The former was from the FRA-JCOPE2 daily data and the latter from hourly data produced by the ocean tide model NAO.99Jb (Matsumoto et al., 2000). Hourly sea-surface height from the Region-1 simulation was used for the Region-2 boundary condition. To generate tidal current radiation through the boundaries, the Flather (1976) method was implemented in the simulations for both regions. Because the present simulations eventually indicated that the tide was an important factor in the heterogeneous sedimentary ^{137}Cs distribution (see discussion in Sect. 4), we attempted to verify the simulated tidal amplitude by comparing to observations (Supplement Fig. S1). However, observations were very limited during the simulation period, because most tidal gauges offshore of east Japan were damaged by the tsunami.

2.3 Seawater ^{137}Cs model

The seawater ^{137}Cs model was used to simulate spatiotemporal variations in dissolved ^{137}Cs , particulate ^{137}Cs , and suspended particulate matter in the seawater. The model was based on the following advection–diffusion–reaction equations that were used in several studies (e.g. Kobayashi et al., 2007; Periañez, 2008; Choi et al., 2013) with the same three-dimensional grid as in the hydrodynamic model:

$$F(C_d) = -\phi k_{1m} C_d + \phi k_{-1} m C_p - \phi \lambda C_d, \quad (1)$$

$$F(m C_p) = \frac{\partial w_p \phi m C_p}{\partial z} + \phi k_{1m} C_d - \phi k_{-1} m C_p - \phi \lambda m C_p, \quad (2)$$

$$F(m) = \frac{\partial w_p \phi m}{\partial z}, \quad (3)$$

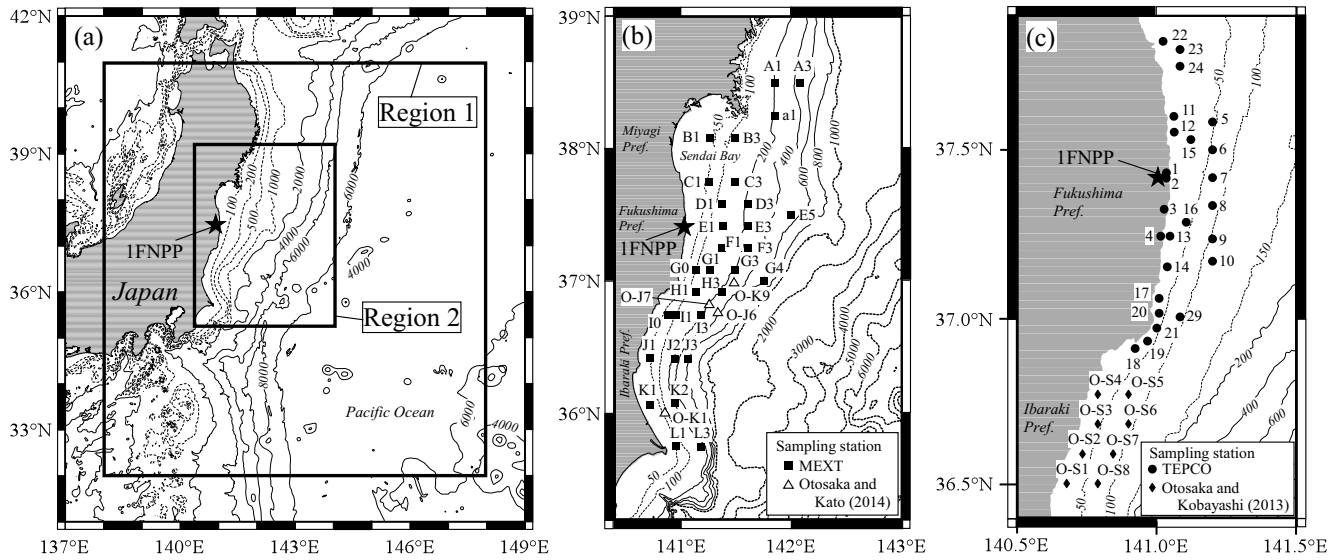


Figure 2. (a) Simulation domain (Region-1 and -2) and locations of sampling stations in (b) MEXT (2011) and Otosaka and Kato (2014) and (c) TEPCO (2011) and Otosaka and Kobayashi (2013). Black star indicates location of 1FNPP. Contours show water depth (m) according to JTOPO30 (MIRC).

where F represents the unsteady advection–diffusion terms, expressed as

$$F(M) = \frac{\partial \phi M}{\partial t} + \frac{\partial u \phi M}{\partial x} + \frac{\partial v \phi M}{\partial y} + \frac{\partial w \phi M}{\partial z} - \frac{\partial}{\partial x} \left(\phi A_x \frac{\partial M}{\partial x} \right) - \frac{\partial}{\partial y} \left(\phi A_y \frac{\partial M}{\partial y} \right) - \frac{\partial}{\partial z} \left(\phi K_z \frac{\partial M}{\partial z} \right); \quad (4)$$

C_d and C_p are activities of the dissolved (Bq m^{-3} -water) and particulate ¹³⁷Cs (Bq kg^{-1} -dry) respectively; m is concentration of the suspended particulate matter (kg-dry m^{-3} -water); w_p represents settling velocities of the suspended particulate matter and particulate ¹³⁷Cs (m s^{-1}); k_{1m} and k_{-1} are kinetic transfer coefficients of adsorption (s^{-1}) and desorption (s^{-1}) respectively; λ is a radioactive decay constant (s^{-1}); u , v and w are three-dimensional seawater currents (m s^{-1}); A_x and A_y are horizontal eddy-diffusion coefficients ($\text{m}^2 \text{s}^{-1}$); K_z is the vertical eddy-diffusion coefficient ($\text{m}^2 \text{s}^{-1}$); ϕ is volumetric seawater content in a simulation grid, as a VOF function ranging from 0 (empty) to 1 (filled) (m^3 -water m^{-3} -grid); volumes of the suspended particulate matter and particulate-¹³⁷Cs are negligible in the seawater. The first term on the right side in Eqs. (2) and (3) indicates settling of the particulate ¹³⁷Cs/suspended particulate matter in the seawater. The second/third terms in Eqs. (1) and (2) represent the rate of ¹³⁷Cs adsorption/desorption on/from the suspended particulate matter. Variables u , v , w , A_x , A_y , K_z , and ϕ were evaluated over time by the hydrodynamic model.

Values of parameters k_{1m} , k_{-1} , and w_p are shown in Table 1. k_{1m} and k_{-1} were derived from other simulations (Periáñez, 2008; Kobayashi et al., 2007). w_p was confirmed as a sensitive parameter for the horizontal dispersion of sedimen-

tary ¹³⁷Cs by our sensitivity analyses. Nevertheless, the value used in other studies (e.g. Kobayashi et al., 2007; Choi et al., 2013) had a wide range ($O(10^{-1}-10^2) \text{ m day}^{-1}$). Although w_p of the fine particulate matter is also known to be variable depending on its concentration (e.g. Sternberg et al., 1999), we treated it as a constant tuning parameter.

Inflow conditions of the dissolved ¹³⁷Cs, particulate ¹³⁷Cs, and suspended particulate matter must be given at the sea-surface boundary in Eqs. (1)–(3) respectively. We considered the ¹³⁷Cs inflow through two pathways: direct discharge from 1FNPP and atmospheric deposition. We treated inflow ¹³⁷Cs as in the dissolved phase. These source data were referred to Tsumune et al. (2012) for time series of direct discharge from 1FNPP (total of 3.5 PBq until the end of May 2011) and Morino et al. (2011) for spatiotemporal variation in atmospheric deposition, simulated by an atmospheric chemical-transport model (total 2.3/1.5 PBq in Region-1/2 through the end of April 2011). However, our preliminary experiments using these data indicated that simulated ¹³⁷Cs activities, especially in surface seawater, were much less than observed in all of Region-2, such that both sources were believed to be underestimated overall. In fact, these amounts were much smaller than a recent evaluation by Miyazawa et al. (2013) (direct discharge 5.5–5.9 PBq through 6 May 2011, atmospheric deposition 5.5–9.7 PBq within 12–62° N and 108–180° E through 6 May 2011). Although their estimation was based on comparison between seawater surface ¹³⁷Cs in their ocean–atmosphere simulations and that of field observations, their oceanic ¹³⁷Cs dispersion model did not include ¹³⁷Cs adsorption on suspended particulate matter and subsequent ¹³⁷Cs sinking in seawater. If downward transport was not negligible, their estimation should in-

Table 1. List of parameter values used in the simulation.

Parameter	Value	Unit	References and other information
Kinetic transfer coefficient of ^{137}Cs desorption	k_{-1}	1.16×10^{-5}	s^{-1} Periañez (2008)
Kinetic transfer coefficient of ^{137}Cs adsorption	k_{1m}	$3.32 \times 10^{-5} m$	s^{-1} = $2m k_{-1}$ (Kobayashi et al., 2007)
Settling velocity	w_p	5.79×10^{-5}	m s^{-1} Tuning
Seabed roughness length	z_0	5.00×10^{-3}	m Standard value
Volumetric water content (porosity)	γ	0.62	$\text{m}^3 \text{m}^{-3}$ e.g. Kusakabe et al. (2013)
Particle density	ρ_p	2.76×10^3	kg m^{-3} Standard value
Dry sediment bulk density	m'	1.05×10^3	kg m^{-3} = $(1-\gamma) \rho_p$
Suspension (erosion) coefficient	E	5.00×10^{-4}	$\text{kg m}^{-2} \text{s}^{-1}$ e.g. Murakami et al. (1989); Blaas et al. (2007)
Critical shear stress	τ_{cr}	0.100	N m^{-2} e.g. Murakami et al. (1989); Blaas et al. (2007)
Sedimentary diffusion coefficient for dissolved ^{137}Cs	D'_d	3.51×10^{-10}	$\text{m}^2 \text{s}^{-1}$ Fossing et al. (2004)
Sedimentary diffusion coefficient for particulate ^{137}Cs	D'_p	3.51×10^{-10}	$\text{m}^2 \text{s}^{-1}$ Fossing et al. (2004)
Decay constant	λ	7.32×10^{-10}	s^{-1} Half-life of 30.2 years

crease. Furthermore, spatiotemporal variation of atmospheric ^{137}Cs deposition over the ocean, which has been estimated by numerical simulation in several studies besides Miyazawa et al. (2013) and Morino et al. (2011), had relatively great uncertainty. These total depositions also had wide variation (e.g. 5 PBq within 30.5–48.0° N, 127.0–154.5° E through the end of April, Kawamura et al., 2011; 7.6 PBq in the North Pacific through the end of April, Kobayashi et al., 2013; 28 PBq in the oceans through 20 April, Stohl et al., 2012). This difference may principally be caused by the source parameter of ^{137}Cs emission from 1FNPP to atmosphere (e.g. 8.8 PBq, Terada et al., 2012; 13 PBq, Chino et al., 2011, 35.9 PBq, Stohl et al., 2012) and wet/dry deposition schemes (e.g. Stohl et al., 2012). The present simulation used source data that were 1.65 times the direct discharge from 1FNPP of Tsumune et al. (2012) and 6.00 times the atmospheric deposition of Morino et al. (2011) (Fig. 3a). As a result, total direct discharge was 5.9 PBq through the end of May. Total atmospheric deposition on the sea surface was 13.8/9.2 PBq in Region-1/2 through the end of April. Although this simple scaling reduced the discrepancy between observed and simulated seawater surface ^{137}Cs , we could not validate the ^{137}Cs inflow conditions in detail because neither the direct discharge nor the atmospheric deposition can be measured directly.

We ignored ^{137}Cs loading from the land as a source because its amount, which has been estimated at 0.0075 PBq of ^{134}Cs , is regarded as nearly equivalent to the ^{137}Cs amount through the end of October 2011 (Otosaka and Kato, 2014). This was much smaller than that of the direct discharge and atmospheric deposition. We also neglected particulate matter loading from the land because of a lack of available data. This may impose some limitation on our simulation, because the validity of that neglect is not well known.

At the bottom boundaries in the seawater ^{137}Cs simulation, diffusion flux of the dissolved ^{137}Cs and sedimentation/suspension fluxes of the particulate ^{137}Cs and suspended particulate matter, which were evaluated by the sediment

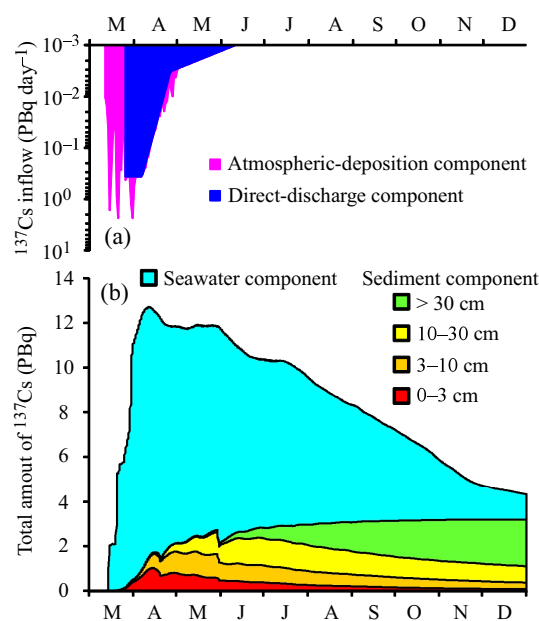


Figure 3. Time series of (a) ^{137}Cs inflow rates of atmospheric deposition and direct discharge from 1FNPP and of (b) total amounts of ^{137}Cs in seawater and sediment over entire simulation domain of Region-2. Both time series are denoted by stacked graph.

^{137}Cs model described in Sect. 2.4, were specified. At the lateral boundaries, the three variables in the Region-1 simulation were set to 0. We used the hourly Region-1 results in the Region-2 domain.

2.4 Sediment ^{137}Cs model

The sediment ^{137}Cs model was used to simulate the vertical ^{137}Cs distribution in the seabed and sedimentation and/or suspension (erosion) at the bottom boundary. This model was based on the vertical one-dimensional transport equations for particulate and dissolved substances in the sediment (e.g. Fossing et al., 2004; Sohma et al., 2008). Lateral transport

into the sediment was negligible. To solve the ¹³⁷Cs transport equations under the sedimentation/suspension conditions, it is necessary to trace the free boundary of the sediment surface, which changes with time on the basis of mass balance of the sedimentary particulate matter. If the usual finite difference method on a Cartesian coordinate (z axis in Fig. 1b) were used, its numerical procedure would be complicated in spite of the idealised sediment. To avoid such complication, we applied a relative vertical coordinate z' , defined as distance from the sediment surface at any time (Fig. 1b). In addition, interaction between the bottom current and topological change of the sediment surface was ignored, and the ideal sediment assumption was used. The vertical transport equations were thus transformed into

$$\gamma \frac{\partial C'_d}{\partial t} + w_s \gamma \frac{\partial C'_d}{\partial z'} = \gamma D'_d \frac{\partial^2 C'_d}{\partial z'^2} - k_{1m} \gamma C'_d + k_{-1} m' C'_p - \lambda \gamma C'_d, \quad (5)$$

$$m' \frac{\partial C'_p}{\partial t} + w_s m' \frac{\partial C'_p}{\partial z'} = m' D'_p \frac{\partial^2 C'_p}{\partial z'^2} + k_{1m} \gamma C'_d - k_{-1} m' C'_p - \lambda m' C'_p, \quad (6)$$

$$m' = (1 - \gamma) \rho_p, \quad (7)$$

where m' is dry sediment bulk density (kg-dry m⁻³-sediment); γ is volumetric water content (m³-porewater m⁻³-sediment), where $(1-\gamma)$ indicates volumetric solid content (m³-solid m⁻³-sediment); ρ_p is particle density (kg-dry m⁻³-particle); C'_d is dissolved ¹³⁷Cs activity in porewater (Bq m⁻³-porewater); C'_p is particulate ¹³⁷Cs activity (Bq kg⁻¹-dry) in the sediment; D'_d and D'_p are diffusion coefficients of the dissolved (m² s⁻¹) and particulate ¹³⁷Cs (m² s⁻¹) in the sediment respectively; and w_s is vertical displacement of the sediment surface per unit time (m s⁻¹). Equation (7) is a stationary solution of the partial-differential transport equation of the particulate matter satisfying the ideal sediment assumption. The second terms on the left side of Eqs. (5) and (6) represent parallel downward/upward translation of the vertical profiles of dissolved and particulate ¹³⁷Cs as much as the sedimentation/suspension thickness (Fig. 1b). Because sediment bulk density and porosity were defined as constant parameters by the ideal sediment assumption, the relationship between the rate of sedimentation/suspension and w_s can be simply expressed by the following linear expression:

$$w_s = (\text{sus}_m - \text{sed}_m) / m', \quad (8)$$

where sus_m and sed_m are suspension (kg-dry m⁻² s⁻¹) and sedimentation (kg-dry m⁻² s⁻¹) fluxes of the particulate matter respectively. They are evaluated by

$$\text{sed}_m = w_p m_b, \quad (9)$$

$$\text{sus}_m = \max [0, E (\tau_b / \tau_{cr} - 1)], \quad (10)$$

where m_b is suspended matter concentration in the bottom seawater (kg-dry m⁻³-water), E is a suspension (erosion) coefficient (kg m⁻² s⁻¹), τ_b is bottom friction (N m⁻²), and τ_{cr} is critical shear stress (N m⁻²). τ_b is calculated using “the law of the wall” from the bottom current (e.g. Deltares, 2012) in the hydrodynamic model, expressed as

$$\tau_b = \rho_b \kappa \Delta z_b (u_b^2 + v_b^2) / \int_0^{\Delta z_b} \ln \left(\frac{z + z_0}{z_0} \right) dz, \quad (11)$$

where ρ_b is bottom seawater density (kg m⁻³-water), κ is the von Kármán constant (=0.4), Δz_b is thickness of the sea-bottom grid (m), u_b and v_b are currents in the x and y directions on the sea-bottom grid (m s⁻¹) respectively, and z_0 is roughness length of the seabed (m). Whereas Eqs. (9) and (10) are simple equations for sediment transport, they have generally been used in studies such as in coastal engineering (e.g. Blas et al., 2007). Sedimentation and erosion of the particulate ¹³⁷Cs are similarly expressed by

$$\text{sed}_m C_p = \text{sed}_m C_{pb}, \quad (12)$$

$$\text{sus}_m C_p = \text{sus}_m C'_{ps}, \quad (13)$$

where $\text{sed}_m C_p$ and $\text{sus}_m C_p$ are sedimentation and suspension rates of the particulate ¹³⁷Cs (Bq m⁻² s⁻¹) respectively and C_{pb} and C'_{ps} are particulate ¹³⁷Cs activity in the bottom seawater (Bq kg⁻¹-dry) and in surface sediment (Bq kg⁻¹-dry) respectively.

A list of parameters in the sediment ¹³⁷Cs model is also given in Table 1. We used k_{-1} and k_{1m} in that model that were identical to those in the seawater ¹³⁷Cs model. These values were confirmed valid by the simulated sedimentary ¹³⁷Cs, which was consistent with little dissolution and nearly irreversible adsorption from and on the sediment in other studies (e.g. Ootosaka and Kobayashi, 2013). The particulate phase (>99% of the sedimentary ¹³⁷Cs) dominated the dissolved phase in the sediment during the simulation term. Sediment physical properties such as particle density, volumetric water content, the suspension coefficient, and critical shear stress were selected as values representative of fine particulate matter (e.g. silt and clay). Sedimentary diffusion coefficients D'_m and D'_p usually consist of molecular diffusion and/or bioturbation (e.g. Fossing et al., 2004; Sohma et al., 2008). These coefficients were taken from the literature (Fossing et al., 2004), but their effects on the simulated result of sedimentary ¹³⁷Cs were found to be slight.

Net flux of particulate ¹³⁷Cs evaluated from Eqs. (12) and (13) was given as the surface seabed condition of Eq. (6) and bottom boundary of Eq. (2). Similarly, net flux of particulate matter from Eqs. (9) and (10) was specified at the bottom boundary in Eq. (3). Exchange of dissolved ¹³⁷Cs between bottom seawater (Eq. 1) and surface seabed (Eq. 5) was calculated from the diffusion equation. The diffusion coefficient was derived from bottom seawater turbulent and sedimentary bioturbation. Adsorption of dissolved ¹³⁷Cs in bottom seawater on surface sediment may occur through the diffusion

process in our model. At the bottom boundaries of Eqs. (5) and (6), we specified flux conditions as advection-outflow at the sedimentation or zero-inflow at the suspension if deeper ^{137}Cs activity was assumed 0. These fluxes were consistent with mass balance of the particulate matter expressed by the identical Eq. (7). However, there is an issue in the method, in that Eq. (7) cannot be restricted to the suspended amount of sediment matter; i.e. it is possible that the fine particulate matter is infinitely and endlessly supplied from deeper levels. Therefore, the present procedure using the relative vertical-axis z' and uniform sediment assumption, which facilitates simulation of the vertical profile of sedimentary ^{137}Cs , probably overestimates the suspension in regions whose seabed does not actually have sufficient suspendible particulate matter.

3 Results

Here we show simulated variation of spatiotemporal ^{137}Cs in both seawater and sediment in Region-2 and describe model performance and uncertainty based on comparison to observation. To evaluate model performance, we used two statistical indexes: factor (FA n) and fractional bias (FB) (e.g. Draxler, 2006; Draxler et al., 2013) as described in Appendix A. FA n is defined as the percentage of number of simulated results within a certain factor n of a measured value (i.e. within a range from n^{-1} - to n -times the measurements). A larger value indicates better estimation. FB represents normalized model bias in a range from -2 to 2 , with positive/negative values indicating overestimation/underestimation. Evaluation results of the statistical indexes for the sea-surface ^{137}Cs , sediment-surface ^{137}Cs , and vertical profile of sedimentary ^{137}Cs are summarised in Supplement Tables S1–S4.

3.1 Seawater ^{137}Cs dispersion

To investigate performance of the seawater ^{137}Cs model, simulated ^{137}Cs activities on the sea surface ($= C_d + mC_p$; however, the sea-surface mC_p was negligible) were compared with observed data. For this comparison, we used TEPCO monitoring data (TEPCO, 2011) at the nearshore sites shown in Fig. 4j, where time series were sufficient. Observations at stations W-1 and W-2 were within the same simulation grid (Fig. 4a and j), because they are very close.

Sea-surface ^{137}Cs simulated by the model largely agreed with observed data (Figs. 4 and S2). The average FA2 at all stations, which had a relatively large value of 52.2%, also indicates good model performance (Table S1). This agreement was mainly attributable to adjustment of the amount of ^{137}Cs inflow through atmosphere deposition and direct discharge from 1FNPP (mentioned in Sect. 2.3). However, all FB values in Table S1 became negative, indicating that the simulations still somewhat underestimated the sea-surface

^{137}Cs . In particular, relatively large discrepancies between the simulations and observations were found in the initial period between the end of March and mid-April (Fig. 4). These discrepancies would affect initial ^{137}Cs sedimentation in the simulation. The results imply that the amount of actual ^{137}Cs inflow exceeded that input to the simulation.

Spatiotemporal variation in sea-surface ^{137}Cs strongly depended on atmospheric deposition prior to the end of March and afterward on direct discharge from 1FNPP (Figs. 3 and 4). Early in April, seawater ^{137}Cs reached a peak $O(10^3 - 10^4)$ Bq L $^{-1}$ along the coast near 1FNPP (Fig. 4a–c) and $O(10^2)$ Bq L $^{-1}$ 15 km offshore (Fig. 4d–i). There was a rapid decline of activity from mid-April to the beginning of May and a gradual decrease afterward (Fig. 4a–i). The decrease in seawater ^{137}Cs was caused by significant dispersion from the coastal region to the open ocean (Fig. S2). As mentioned in Sect. 1, many studies have discussed the spatiotemporal ^{137}Cs distribution and its detailed physical background on the basis of numerical simulations (Kawamura et al., 2011; Tsumune et al., 2012, 2013; Masumoto et al., 2012; Choi et al., 2013; Miyazawa et al., 2012, 2013). Hence, we do not address the seawater ^{137}Cs in detail hereafter. It stands to reason that there was no earlier simulation that quantitatively agreed with our spatiotemporal distribution of seawater ^{137}Cs because of differences in numerical procedures and/or simulation conditions. Thus, we confirmed that our seawater ^{137}Cs dispersion (Figs. 4 and S2) had qualitative features similar to the earlier simulations. For instance, our simulation tended to underestimate sea-surface ^{137}Cs southeast of 1FNPP, such as at stations W-8 through W-10 (Fig. 4g–i and FB in Table S1) per the earlier simulations (Kawamura et al., 2011; Tsumune et al., 2012; Miyazawa et al., 2013).

3.2 Spatiotemporal ^{137}Cs distribution on surface of sediment

To evaluate the reproduction performance of the sediment ^{137}Cs model, simulated ^{137}Cs on the sediment surface was compared with observations (Figs. 5–7 and Tables S2 and S3). We mainly used sediment sampling data from the Ministry of Education, Culture, Sports, Science and Technology (MEXT) and TEPCO. TEPCO sampling stations were near the shore of Fukushima Prefecture (Fig. 2c), and MEXT monitoring stations were offshore of Miyagi through Ibaraki Prefectures (Fig. 2b). Detailed information on MEXT measurements was given by Kusakabe et al. (2013). It was noted that TEPCO data were published in units Bq kg $^{-1}$ -wet at the time, while others were in Bq kg $^{-1}$ -dry.

Spatiotemporal variations of the sediment-surface ^{137}Cs were comparable with the observations in both coastal and offshore regions (Figs. 5–7). Station averages of FA2, which are 40.7% for the offshore MEXT stations (Table S2) and 30.1% for the coastal TEPCO stations (Table S3), indicate tolerable model performance. Simulated sediment-surface ^{137}Cs activities increased dramatically in the first 3 months

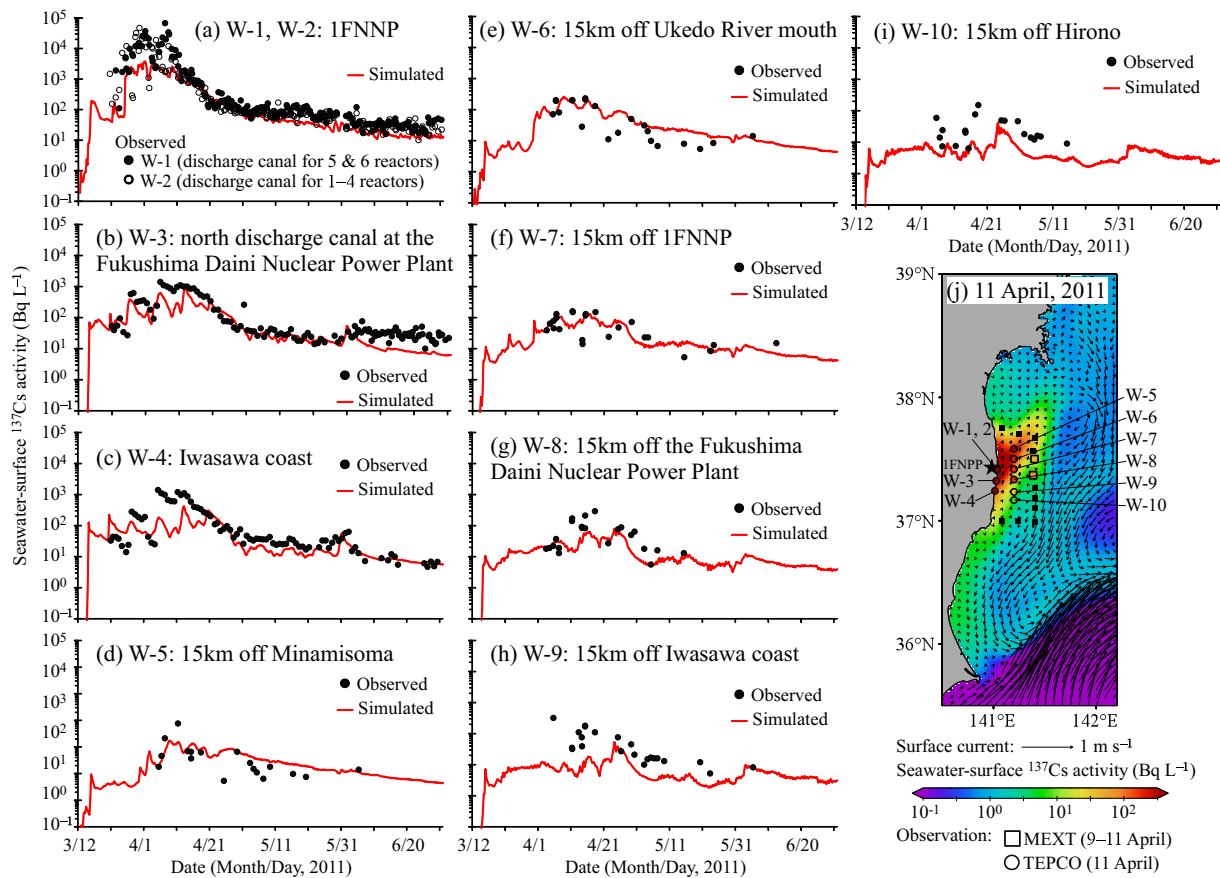


Figure 4. (a)–(i) Time series of observed and simulated seawater-surface ^{137}Cs at TEPCO (2011) stations W-1 through W-10. (j) Location of the stations and an example of spatial distributions in observed (colour square plot) and simulated ^{137}Cs (colour shading) on sea surface (11 April 2011). Arrows show daily-mean current on sea surface. Black star indicates location of 1FNPP. Black square plots indicate observations of non-detected seawater ^{137}Cs activities.

at most of the stations (Figs. 6 and 7) but, unfortunately, this cannot be sufficiently verified because of a lack of observations during that period. Afterward, activities remained stable or decreased steadily. These temporal changes in sediment-surface ^{137}Cs activities indicate that reproduction performance for the sediment-surface ^{137}Cs was largely determined by the initial ^{137}Cs migration from seawater to seabed.

The simulation overestimated some sediment-surface ^{137}Cs activities, especially in the region northeast of 1FNPP such as at MEXT stations B1 and C1 (Fig. 6b and c) in Sendai Bay and TEPCO stations 5 and 6 (Fig. 7d) near the coast of northern Fukushima where even FA5 values were 0.0 % (Tables S2 and S3). It was believed that the main cause of these overestimations was the uniform application of the ideal sediment assumption to the entire simulation domain. As mentioned in Sect. 2.4, our model possibly overestimated the amount of particulate matter suspended from the seabed, especially in regions whose sediment does not actually have sufficient suspendible particulate matter. The suspended particulate matter is important in ^{137}Cs migration from seawater to seabed in our model, because ^{137}Cs in seawater cannot

sink toward the bottom unless it is transformed from dissolved to particulate phase by adsorbing on the suspended particulate matter (Fig. 1a). Hence, it is believed that the excess particulate matter suspended from the seabed resulted in overestimation of the sediment-surface ^{137}Cs . Indeed, the region where the simulation overestimated sediment-surface ^{137}Cs was dominated by coarse sand outcrops in surveys prior to the powerful tsunami (Aoyagi and Igarashi, 1999). In addition, sediment sampling after the tsunami indicated that the surface sediment had low water contents, which correspond to coarse particles at MEXT stations B1 and C1 (Kusakabe et al., 2013).

Despite the aforementioned limitation, our model succeeded in reasonably reproducing the hotspot swath (Fig. 5j), consistent with the recent observations (Thornton et al, 2013; Ambe et al., 2014) described in Sect. 1. The hotspot swath could not be captured by the sediment sampling with coarse spatial resolution, such as that of TEPCO (2011) and MEXT (2011), as mentioned in Sect. 1. The ability to simulate such a heterogeneous distribution of sedimentary ^{137}Cs was very interesting and valuable, because the simulation

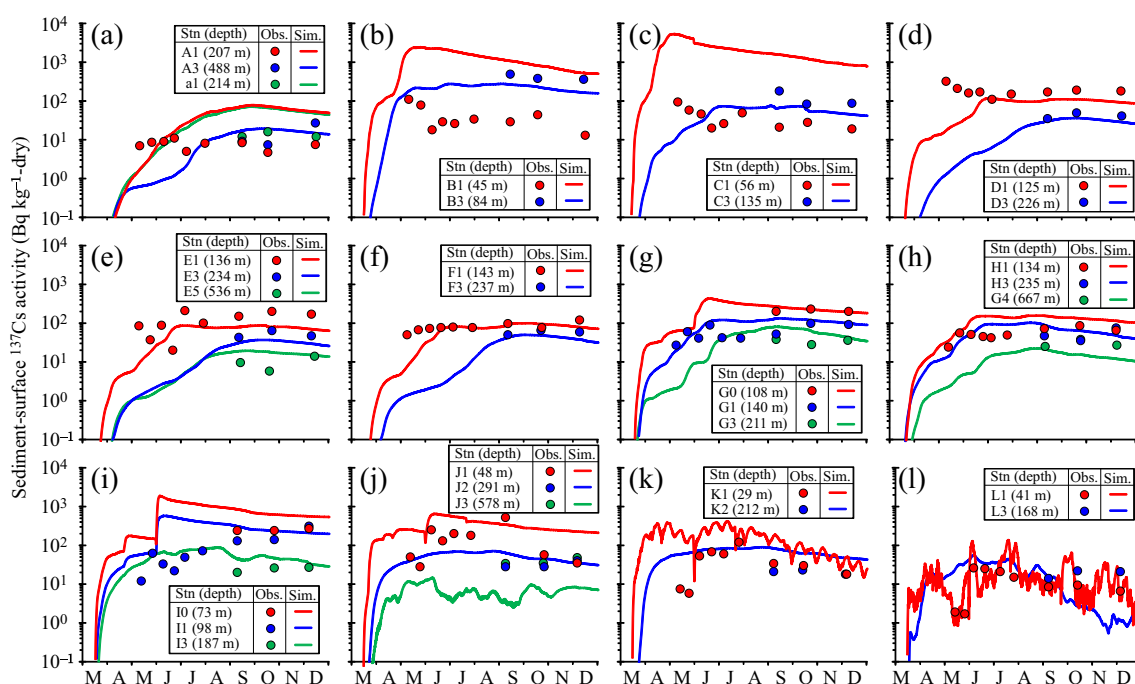


Figure 6. Time series of observed (circular plots) and simulated (lines) sediment-surface ^{137}Cs at MEXT (2011) stations. Locations of observations are shown in Fig. 1b. Water depths are according to Kusakabe et al. (2013).

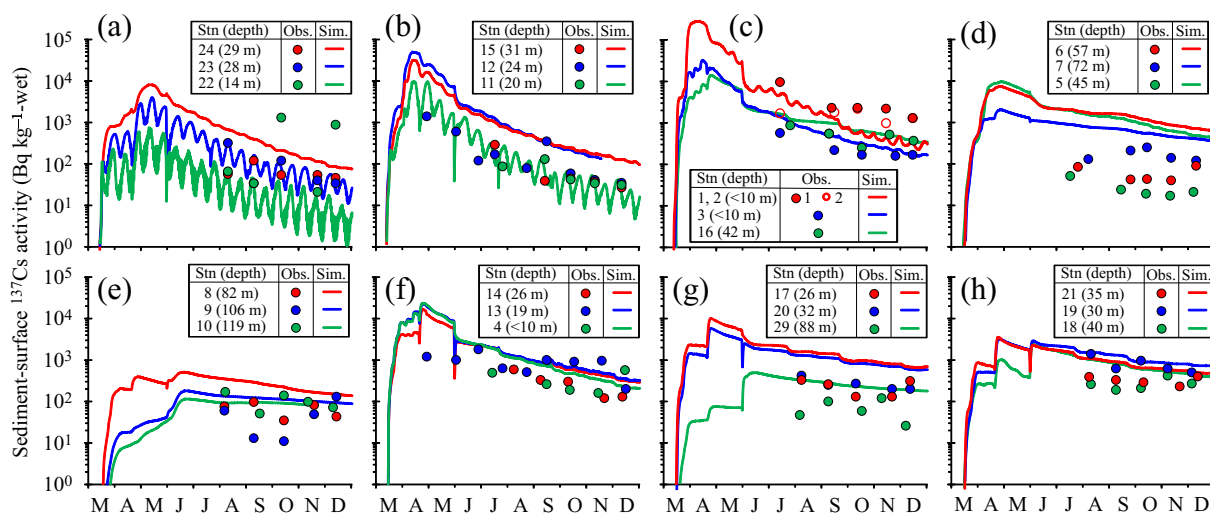


Figure 7. Time series of observed (circular plots) and simulated (lines) sediment-surface ^{137}Cs at TEPCO (2011) stations. Locations of observations are shown in Fig. 1c. Longitude axis has units $\text{Bq kg}^{-1}\text{-wet}$. Water depths are according to JTOPO30 (MIRC).

used the ideal sediment assumption over the entire simulation domain. That is, spatial distributions of sediment adsorptivity with caesium input data were not input to the model, in contrast to the simulation of Misumi et al. (2014). Sequential processes causing the hotspot swath simulated by our model are discussed in detail in Sect. 4.

3.3 Vertical ^{137}Cs profile in sediment

It is important to understand the performance and uncertainty of our sediment ^{137}Cs model by comparing observed and simulated vertical profiles of sedimentary ^{137}Cs . However, we could not accomplish this adequately, because there were only a few data available in the study area in 2011. Among those, we used observations of Otosaka and Kobayashi (2013) and Otosaka and Kato (2014). The for-

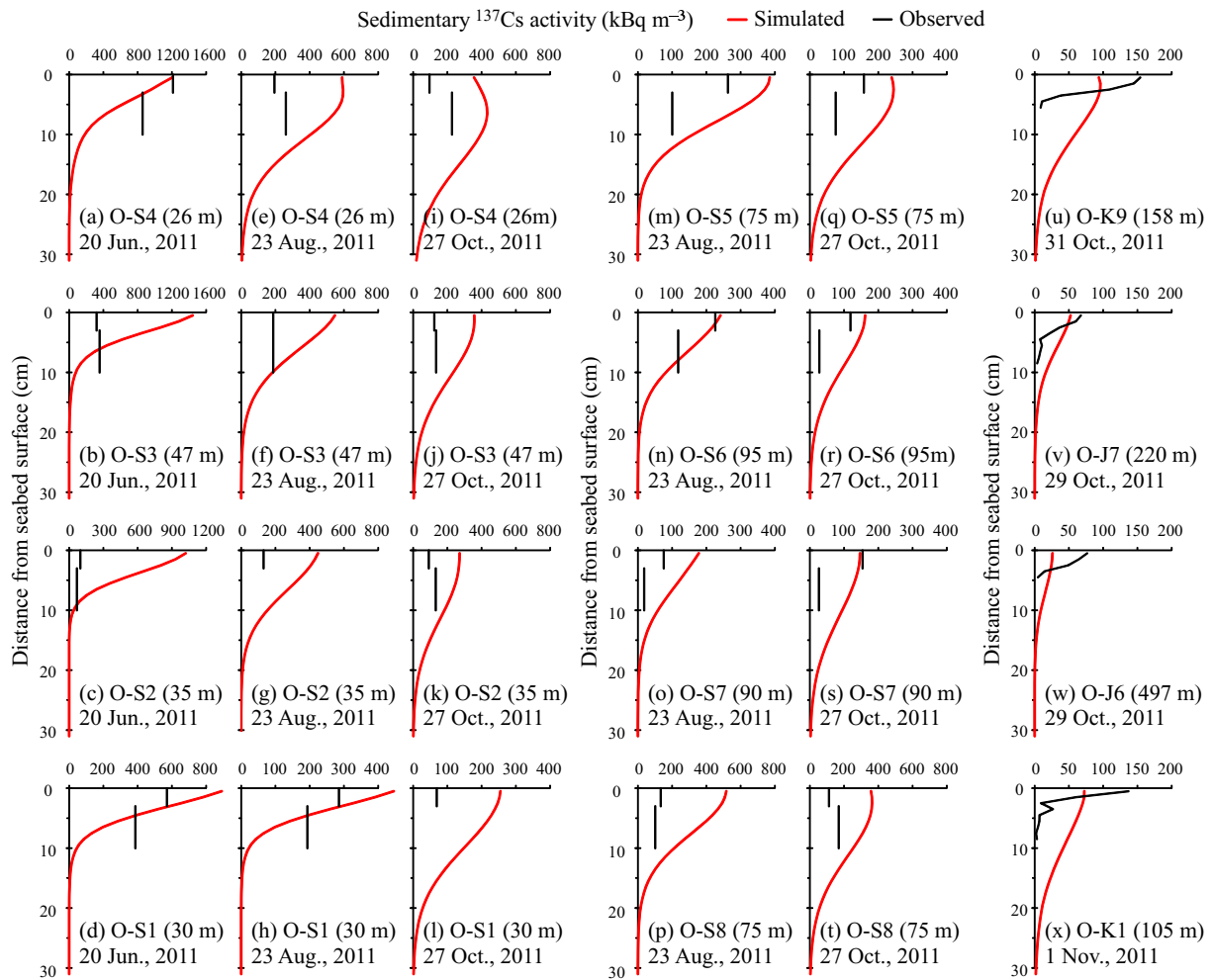


Figure 8. Comparison between simulated vertical sedimentary ^{137}Cs profiles (red lines) and observed (black lines) by (a–t) Otosaka and Kobayashi (2013) and (u–x) Otosaka and Kato (2014). Values in parentheses show observed water depth.

mer were from a narrow nearshore region (26–95 m depths) off Ibaraki Prefecture (Fig. 2c). Their samples were from the upper 10 cm of sediment and cut into two layers, upper (0–3 cm) and lower (3–10 cm). The latter sampling stations were offshore (105–1175 m depths) of Fukushima and Ibaraki prefectures, and samples were upper from 10 cm of sediment and cut into 1 cm thick sections. Although the latter survey was over a wider area than the former, we selected observations at only four stations (Fig. 2b) where sedimentary ^{137}Cs concentration $m'C'_p$ was considerably greater than 50 kBq m^{-3} . It is an issue that the above two observations covered only a small part of Region-2, not including notable regions such as the nearshore off 1FNPP and Sendai Bay.

The comparison in the nearshore region off Ibaraki Prefecture (Fig. 8a–t) indicates that simulated sedimentary ^{137}Cs in the upper 3 cm layer largely agreed with the observations within one order of magnitude. The station-average FA5 is 95.0 %, also showing good model performance, but the station-average FB is a positive value of 0.72, indicat-

ing some overestimation (Table S4a). Discrepancy between simulated and observed sedimentary ^{137}Cs in the lower layer (3–10 cm) was less than that in the upper layer; station averages of FA2 and FB in the lower layer were superior to those in the upper layer (Table S4a). By contrast, results in the offshore region (Fig. 8u–x and Table S4b) show that our model clearly overestimated sedimentary ^{137}Cs in the lower layers (4–30 cm), although the simulated result in the upper layers (0–4 cm) agreed well with the observations. In particular, at the Otosaka and Kato (2014) stations O-K9 and O-K1, simulated sedimentary ^{137}Cs dispersion into the sediment reached about 20 cm depth, although observation was confined to 5 cm depth (Fig. 8u, x). Although these results imply that sedimentation of the suspended matter and particulate ^{137}Cs were somewhat overestimated in the offshore region by our model, this did not matter much because the sedimentary ^{137}Cs amounts were very small there.

Notably, the simulation successfully reproduced an observed feature of the vertical sedimentary ^{137}Cs profile, i.e.

activity in the deeper sediment was significantly higher than that in the upper in the nearshore region, such as at the Otsuka and Kobayashi (2013) station O-S4 (Fig. 8i). Processes causing such a vertical profile in the sediment are described in Sect. 4.2.

4 Discussion

4.1 Total amount of sedimentary ¹³⁷Cs and its uncertainty

The total ¹³⁷Cs amount rapidly increased at the beginning of April in our simulation because of atmospheric deposition and direct discharge from 1FNPP (Fig. 3). After that, it stabilised at ~ 12 PBq by the end of May and strongly declined to 4.3 PBq at the end of 2011. The latter decrease was caused by the seawater ¹³⁷Cs dispersed from Region-2 to the open ocean. Sedimentary ¹³⁷Cs also increased steadily until onset of the significant seawater dispersion but suddenly declined at the end of May. This rapid decrease resulted from short but strong suspension induced by an extratropical cyclone that originated as typhoon 201102 (SONGDA) and passed over the southern part of Region-2. Afterward, the sedimentary ¹³⁷Cs rapidly recovered, indicating that the suspended ¹³⁷Cs returned to the sediment. Such behaviours of sedimentary ¹³⁷Cs before and after the cyclone were also simulated by Choi et al. (2013).

In our simulation, total sedimentary ¹³⁷Cs was 0.10 PBq (0.66 % of total ¹³⁷Cs inflow) in the upper 3 cm layer, 0.40 PBq (2.6 % of total ¹³⁷Cs inflow) in the upper 10 cm layer, and 3.2 PBq (21 % of total ¹³⁷Cs inflow) in the entire seabed over all of Region-2 (1.4 × 10⁵ km²) at the end of 2011. Kusakabe et al. (2013) estimated 0.042–0.052 PBq of total sedimentary ¹³⁷Cs between September and December 2011 in the upper 3 cm seabed off Miyagi, Fukushima, and Ibaraki prefectures (2.2 × 10⁴ km² domain) on the basis of the MEXT (2011) observations. Otsuka and Kato (2014) estimated total sedimentary ¹³⁴Cs. This was regarded as nearly equivalent to ¹³⁷Cs amount at 0.20 ± 0.06 PBq (decay corrected to 11 March 2011) within the region less than 200 m depth (1.5 × 10⁴ km² domain) in October 2011, using their sampling data in upper 10 cm sediments and MEXT observations. Accounting for the difference in study area, our results of sedimentary ¹³⁷Cs amounts in the upper layers were almost comparable to the two studies above. However, the simulated amounts in the upper 3 and 10 cm layers were only 3 and 13 % of total sedimentary ¹³⁷Cs respectively; the remainder was present in deeper sediment.

We could not adequately validate the simulated result of large ¹³⁷Cs amount in the deeper layers. One of the reasons was a lack of observations in deeper sediment, necessary for validation after the accident, especially near 1FNPP where massive sedimentary ¹³⁷Cs remains even today (described in Sect. 3.3). We described in Sect. 3.2 that the simu-

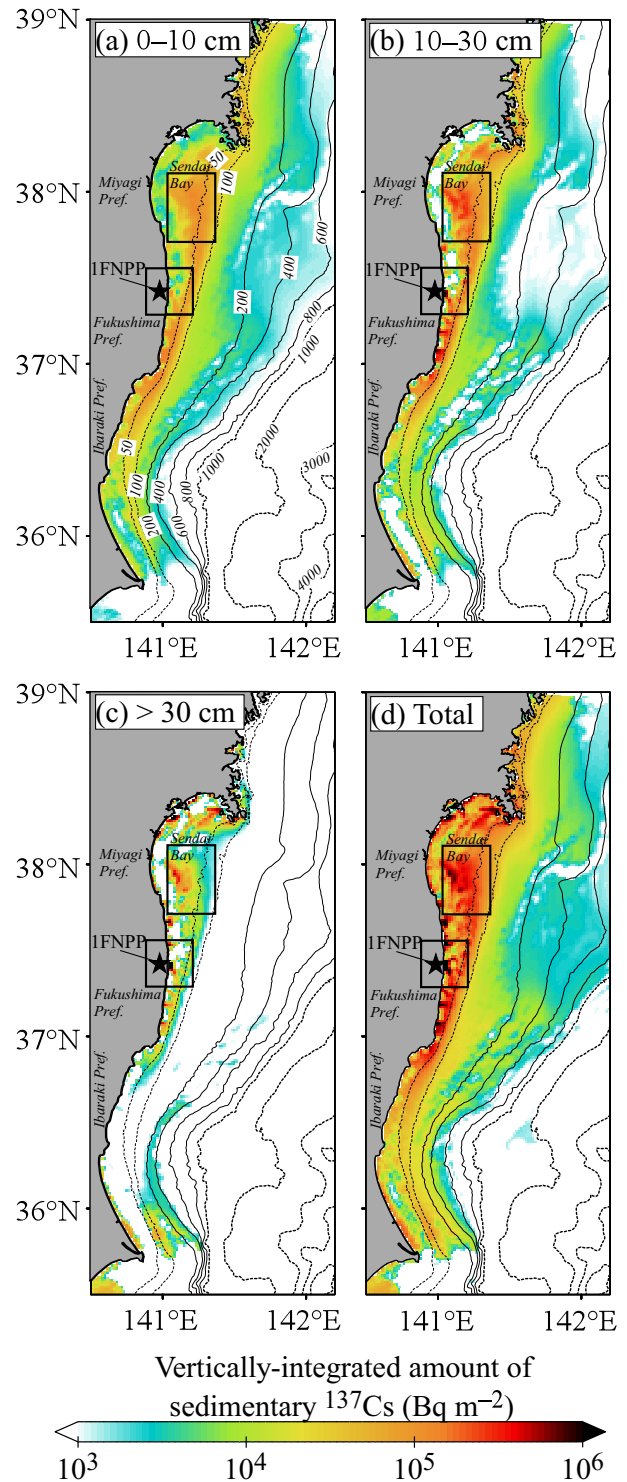


Figure 9. Simulated vertically integrated amounts of sedimentary ¹³⁷Cs at the end of 2011 in the (a) surface (0–3 cm) layer, (b) upper 10–30 cm layer, (c) >30 cm deep layer, and (d) vertical-total sediment. Black star indicates location of 1FNPP. Contours show water depth (m) according to JTOPO30 (MIRC). Rectangular regions are cited in Sect. 4.1.

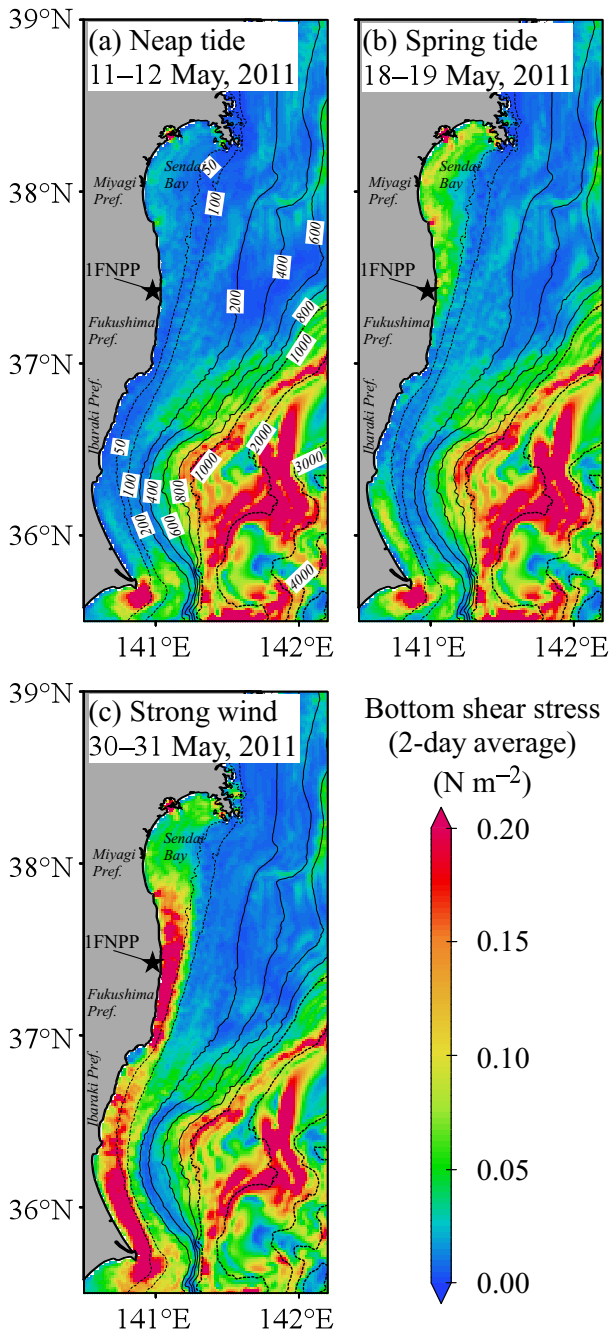


Figure 10. Simulated spatial distributions of 2-day averages of bottom shear stress for events of (a) spring tide (11–12 May 2011), (b) neap tide (18–19 May 2011), and (c) strong wind (30–31 May 2011). Black star indicates location of 1FNPP. Contours show water depth (m) according to JTOPO30 (MIRC).

lated concentrations of sediment-surface ¹³⁷Cs were roughly comparable with observations except for overestimation to the northeast of 1FNPP. However, this agreement could not validate ¹³⁷Cs migration flux from seawater to sediment. The insufficiency of deeper data was also the reason why

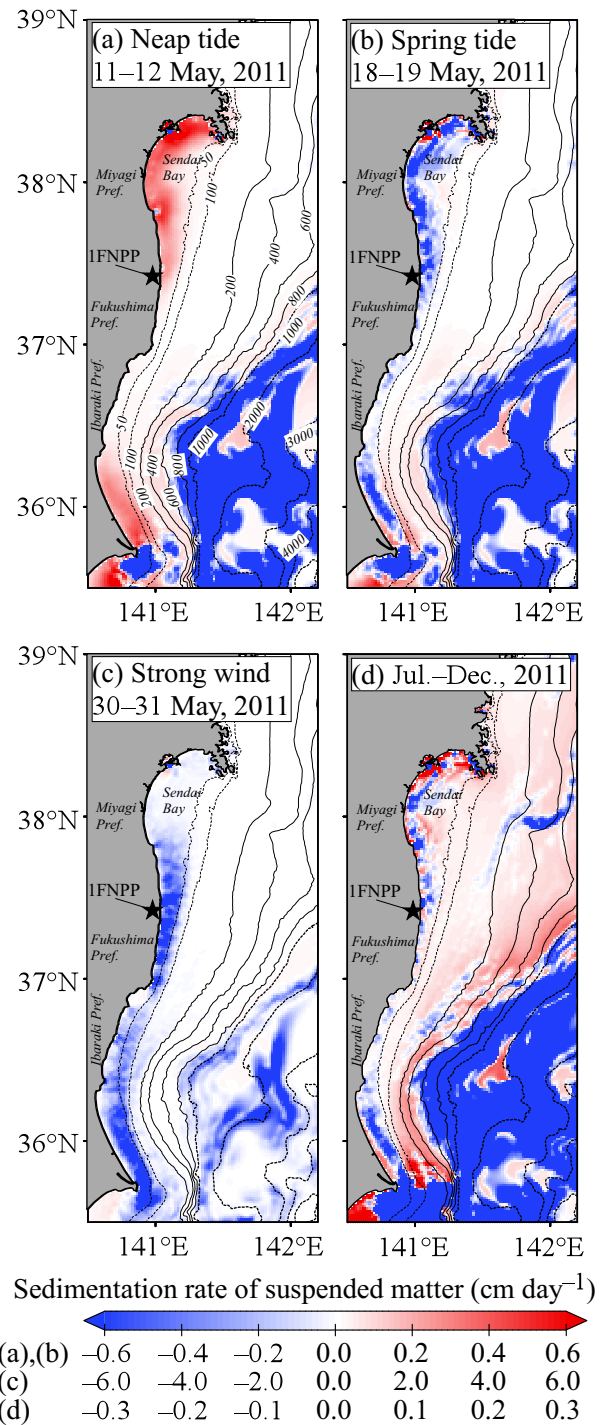


Figure 11. Simulated spatial distributions of 2-day average sedimentation rates of suspended matter for events of (a) spring tide (11–12 May 2011), (b) neap tide (18–19 May 2011), and (c) strong wind (30–31 May 2011). (d) Long-term average sedimentation rates of suspended matter from July through December 2011. Black star indicates location of 1FNPP. Contours show water depth (m) according to JTOPO30 (MIRC).

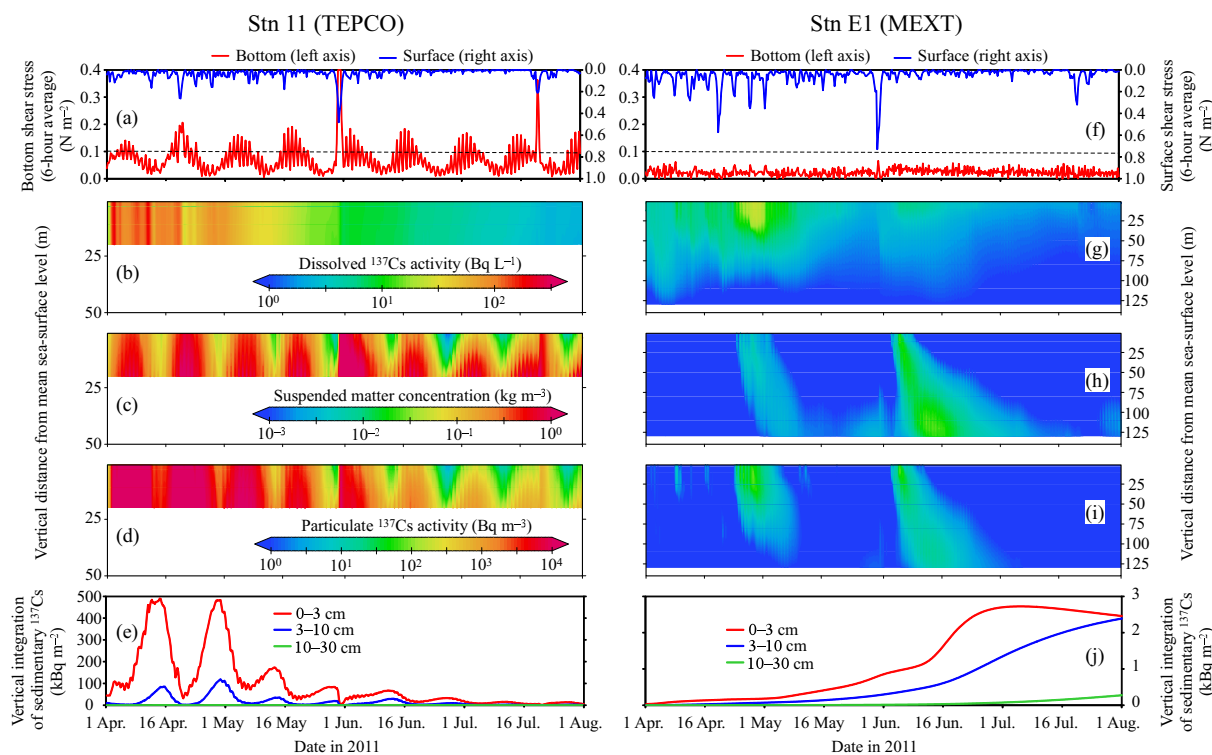


Figure 12. (a) Bottom shear stress and surface shear stress; (b–d) vertical profiles of dissolved ^{137}Cs activity, suspended matter concentration, and particulate ^{137}Cs activity in seawater respectively; (e) vertical integration of sedimentary ^{137}Cs at shallow site (TEPCO station 11 in Fig. 2c). (f–j) Same as (a–e) but at offshore site (MEXT station E1 in Fig. 2b).

the earlier estimations of total sedimentary ^{137}Cs might be underestimated as described by their authors (Kusakabe et al., 2013; Otosaka and Kato, 2014). Indeed, recent surveys have detected high-activity $O(10^3\text{--}10^4)\text{ Bq kg}^{-1}$ ($= O(10^6\text{--}10^7)\text{ Bq m}^{-3}$) through the present in both surface and lower ($> 30\text{ cm}$) sediment at several sampling stations near 1FNPP (Thornton et al., 2013; NRA, 2014a). Our simulation also revealed 1.0 PBq (31 % of total sedimentary ^{137}Cs) in a large amount of sedimentary ^{137}Cs in the $30 \times 30\text{ km}$ square domain ($140.88\text{--}141.21^\circ\text{ E}$, $37.29\text{--}37.56^\circ\text{ N}$ in Fig. 9, except for the land) around 1FNPP at the end of 2011.

Another reason why we could not validate the sedimentary ^{137}Cs amount in the deeper layer was uncertainty related to our simulation conditions. As mentioned in Sect. 2.4, because we used the ideal sediment assumption, our simulation would overestimate sedimentary suspension unless the actual seabed consisted mainly of fine particles. In fact, that simulation overestimated some sediment-surface ^{137}Cs activities to the northeast of 1FNPP and Sendai Bay, whose seabed was dominated by coarse sand (mentioned in Sect. 3.2). The simulated amount of sedimentary ^{137}Cs in the $30 \times 45\text{ km}$ rectangular region in Sendai Bay ($141.03\text{--}141.37^\circ\text{ E}$, $37.71\text{--}38.11^\circ\text{ N}$ in Fig. 9) reached 0.52 PBq (16% of total sedimentary ^{137}Cs). Furthermore, our result included uncertainty of ^{137}Cs inflow conditions, especially the atmospheric depo-

sition (Sect. 2.2). Clearly, the total amount of sedimentary ^{137}Cs directly depends on that of ^{137}Cs inflow.

4.2 Influences of tide and strong wind on sedimentary ^{137}Cs on shallow shelf

Suspension of particulate matter from the seabed was important in determining spatiotemporal variation of sedimentary ^{137}Cs in our model, as mentioned in Sect. 3.2. This significant suspension is generally induced by strong bottom friction, caused by ocean currents, tides, wind waves, and others. From linear long-wave theory, current velocity is in inverse proportion to the square root of water depth; thus, influences such as tide and wind on bottom shear stress tend to increase with water depth (but also depend on local bottom topography of course). Our simulation confirmed that strong bottom friction exceeding the critical shear stress (0.10 N m^{-2} in the simulation) in the shallow region ($< 50\text{ m}$ depths) tended to occur more frequently than offshore ($50\text{--}200\text{ m}$ depths) (Fig. 10). Extremely strong bottom friction is also found in the deep region ($> 800\text{ m}$ depths) (Fig. 10). This is caused by the strong Kuroshio Current. As a result, sediment suspension occurred there at all times in our simulation (Fig. 11). This simulated result was probably in disagreement with actual suspension there. However, the direct effect of this on the simulated ^{137}Cs behaviour in and around the shelf re-

gion (<200 m depths), such as sedimentary ^{137}Cs activity, was slight. This was because particulate matter suspended from the deep sediment had difficulty being transported upward beyond several tens of metres above the seabed by vertical mixing. Therefore, this suspended matter rapidly settled on the seabed within the deep region or dispersed to the open ocean because of the Kuroshio Current in our simulation (no figure shown).

The simulation indicates that the tide caused significant suspension and sedimentation of the particulate matter in the nearshore region from Sendai Bay to 1FNPP and off southern Ibaraki (Figs. 10a and b and 11a and b). Bottom friction in the nearshore region varied periodically, and the variation period of strong bottom friction exceeding the critical shear stress was approximately 2 weeks, corresponding to the spring–neap tidal variation (Fig. 12a). The same periodic changes were found in temporal variations of the vertical profiles of suspended matter concentration and particulate ^{137}Cs activity in seawater above the seabed (Fig. 12c and d). The simulated results revealed that this tidal bottom disturbance caused suspension during spring tide and sedimentation during neap tide (Fig. 11a and b). Particulate matter and particulate ^{137}Cs suspended from the seabed were not believed to be transported over a large horizontal scale, because they rapidly settled on the bottom for several days (Fig. 12c and d). However, the long-term periodic tidal disturbance made the suspension/sedimentation distribution heterogeneous (Fig. 11d). We also found similar periodic changes in simulated sediment-surface ^{137}Cs activities at some nearshore TEPCO stations (Figs. 7a, b and c and 12e). It is believed that these temporal changes – perhaps including observed ones as at TEPCO station 22 (Fig. 7a) – resulted from the periodic tidal disturbance. In addition, this long-term tidal influence steadily and strongly reduced sediment-surface ^{137}Cs activities (Figs. 7a, b, c, f, and 12a), whose rate of decrease tended to be greater in the shallower region. Periañez et al. (2012) indicated little tidal effects on the initial ^{137}Cs dispersion and sedimentation on the basis of their numerical experiments, but our simulation suggests that this finding should be confined to the initial 3 months after the accident, and that the tide is very important for long-term sedimentary ^{137}Cs behaviour in the shallow region.

Strong wind also had considerable but occasional impacts on the bottom in the shallow region. In particular, the extratropical cyclone at the end of May increased the bottom shear stress to well beyond the critical value (Fig. 10c). As a result, simulated sediment-surface ^{137}Cs activities at many stations near 1FNPP (e.g. TEPCO stations 1, 2, 4, 11, 14, and 20–23 in Fig. 7) suddenly decreased about an order of magnitude. As mentioned in Sect. 3.1, the suspended ^{137}Cs rapidly returned to the seabed afterward, across all of Region-2 (Fig. 3). However, the sediment-surface ^{137}Cs activities did not necessarily return to levels before the strong wind event (TEPCO stations 1, 2, and 4 in Fig. 7). On the contrary, we found that the latter sediment-surface ^{137}Cs be-

came much greater than before at some sites (TEPCO stations 18 and 29 in Fig. 7). These results suggest that the strong wind event considerably enhanced horizontal transport of sedimentary ^{137}Cs and bottom suspension.

The bottom disturbance caused by the tide or strong wind did not occur in every shallow region (<50 m depths) because of the seabed topography and other factors. In the narrow nearshore region from south Fukushima to north Ibaraki, bottom friction did not increase even during extratropical cyclone passage (Fig. 10c). The Otosaka and Kobayashi (2013) station O-S4, where apparent downward movement of sedimentary ^{137}Cs was found in both observation and simulation (Fig. 8i), was located just in that region. This area was where the bottom disturbance rarely occurred; if anything, the sedimentation slightly dominated the suspension over a long period (Fig. 11d). This indicates that the apparent vertical transport of sedimentary ^{137}Cs found at station O-S4 was caused by relatively fresh suspended particulate matter settling on earlier sediment containing substantial ^{137}Cs . It is inconceivable that the amount of sedimentation over only several months became so large under the stable seabed condition. Although this is probably caused by the uncertainty related to the ideal sediment assumption as mentioned in Sect. 4.1, this may have been possible in the unstable seabed state just after the extraordinary disturbance of the tsunami.

4.3 Sedimentary ^{137}Cs behaviour in offshore region

In contrast to the shallow region, in the offshore region along the shelf break (50–200 m depths), impacts of the tide and strong wind on the bottom disturbance were much weaker (<50 m depths). Even the extratropical cyclone that caused the strong bottom disturbance in the shallow region at the end of May could not increase bottom friction beyond the critical shear stress (Figs. 10c and 12f), so little sediment was suspended (Figs. 11c and 12h). Although strong vertical mixing then occurred in seawater, dissolved ^{137}Cs activity in bottom seawater did not increase (Fig. 12g), in contrast to the shallow result (Fig. 12b). Nevertheless, sedimentary ^{137}Cs activities in the offshore region began to increase significantly just after that strong wind event (MEXT stations C3, E1, D1, G0, G1, I0, I1, J1 in Fig. 6, and E1 in Fig. 12j). This increase in sedimentary ^{137}Cs resulted from sedimentation of particulate ^{137}Cs (Fig. 12i), which was suspended and horizontally transported into and from the adjacent shallow shelf by the wind event. This horizontal transport is supported by the fact that both concentrations of suspended matter and particulate ^{137}Cs suddenly increased in the upper seawater, without bottom suspension or upward diffusion (Fig. 12h and i).

The bottom friction barely exceeded the critical shear stress caused by the spring–neap tidal variation in the offshore region as well (Figs. 10 and 12f). Hence, the particulate ^{137}Cs , once settled on the seabed, was rarely moved horizontally over a long period. This result is consistent with the fact that both simulated and observed sediment-surface

^{137}Cs at many offshore stations remained stable or slightly decreased after the strong sedimentation during extratropical cyclone passage (Figs. 6 and 12j). Although there were considerable changes in sediment-surface ^{137}Cs at MEXT offshore stations J3 and L3 (Fig. 6j and l), this was because of seasonal variation in strong bottom disturbance caused by the Kuroshio Current.

4.4 Hotspot swath

The hotspot swath in our simulation was just offshore of the shelf break (along the 50–100 m isobath) off southern Fukushima Prefecture through northern Sendai Bay at the end of 2011 (Fig. 5j). After the 1FNPP accident, the region of high sedimentary ^{137}Cs activity gradually expanded from south of 1FNPP to north in and around the shelf (< 100 m depths) by June (Fig. 5a–e). Afterward, in the shallow shelf (< 50 m depths), the sediment-surface ^{137}Cs significantly decreased because of the periodic tidal disturbance causing sediment suspension, horizontal transport in the seawater, and/or apparent downward movement in the seabed. Meanwhile, in the offshore region (50–100 m depths), the sedimentary ^{137}Cs that settled after being horizontally transported from the shallow region during the extratropical cyclone at the end of May remained largely stable because of rare bottom disturbance. The present simulation suggests that these were the sequential processes causing the hotspot swath and that its shape is closely related to spatiotemporal variation between bottom shear stress on the shallow shelf and that offshore of the shelf break. Although our simulation includes quantitative uncertainty as mentioned in Sect. 4.1, these processes are at least qualitatively reasonable. This is because ^{137}Cs accumulation in the hotspot swath is governed mainly by ocean dynamics, i.e. spatiotemporal variation of bottom shear stress. That is, the quantitative uncertainty in simulation conditions would affect amounts of suspension and subsequent horizontal transport of sedimentary ^{137}Cs on the shallow shelf but not the ^{137}Cs accumulation location offshore.

As mentioned in Sect. 1, Misumi et al. (2014) developed a sediment-surface ^{137}Cs model by considering the spatial distribution of sedimentary adsorptivity with caesium. They thereby reproduced the spatially heterogeneous distribution in sediment-surface ^{137}Cs , as in our simulation. Although the processes causing this distribution in their simulation appeared distinct from those in ours, they were not unrelated. This was because the ease/difficulty of sedimentation and accumulation of suspended particulate matter with high adsorptivity were related to the rare/frequent occurrence of strong bottom friction (Figs. 10 and 11). It is believed that our successful reproduction of the hotspot swath resulted from rough consistency between the actual distribution of seabed properties (e.g. Aoyagi and Igarashi, 1999) and the simulated spatial variation of bottom friction.

5 Conclusions

To clarify ocean dynamic processes causing the massive heterogeneous sedimentary ^{137}Cs distribution that persists in and around the shelf off Fukushima and adjacent prefectures, we numerically simulated oceanic ^{137}Cs behaviour for about 10 months after the 1FNPP accident. We succeeded in simulating that distribution, especially the hotspot swath just offshore of the shelf break (along the 50–100 m isobath) shown by recent observations (Thornton et al., 2013; Ambe et al., 2014; NRA, 2014a). However, quantitative validation of sedimentary ^{137}Cs amount was inadequate. The result suggests that several spatiotemporal characteristics of the sedimentary ^{137}Cs are produced by ocean dynamics.

The simulation provided new and meaningful findings to help predict the sedimentary ^{137}Cs fate. The most important suggestion is that the shape of the hotspot swath is largely due to spatiotemporal variation between bottom shear stress in the shallow shelf and that offshore of the shelf break, corresponding to regional-scale bathymetry. Although sediment in the hotspot swath consists of fine particulate matter with high caesium adsorptivity (Thornton et al., 2013; Ambe et al., 2014; NRA, 2014a), the shape of the swath is not directly attributable to that caesium adsorptivity of the sediment. Our simulation indicated that sediment with sufficient fine particulate matter resulted only from the fact that this matter was horizontally transported from the adjacent shelf and readily settled there. It was also found that the accumulation process of sedimentary ^{137}Cs in the hotspot swath was the same as that of the particulate matter. These results indicate that this swath was where the particulate matter (incorporated with ^{137}Cs) was readily accumulated, because it was in a boundary region between frequent and rare occurrence of bottom disturbance caused by tides and/or strong wind. It is therefore predicted that large amounts of sedimentary ^{137}Cs that are currently in the hotspot swath will remain stable or be submerged by additional sedimentation of fresh particulate matter.

Our simulation also produced significant findings regarding sedimentary ^{137}Cs behaviour on the shallow shelf. There, the simulated bottom disturbance tended to occur frequently because of the periodic spring tide and occasional strong winds, steadily decreasing simulated sediment-surface ^{137}Cs per several observations. The simulation indicated that repeated bottom disturbances reducing sediment-surface ^{137}Cs over the long term caused sedimentary ^{137}Cs to not only be horizontally transported to the offshore region but also vertically toward deeper sediment. Consequently, in our simulation, relatively large amounts of ^{137}Cs in deeper sediment remained on the shallow shelf, especially near 1FNPP, even about 10 months after the 1FNPP accident. Hence, total sedimentary ^{137}Cs at the end of 2011 reached 3.2 PBq, and 87 % of that was present below the 10 cm layer. If our simulation is correct, ^{137}Cs in deeper sediment would be much greater than in upper sediment and would remain stable over a long

period. However, the simulated sedimentary ^{137}Cs amount in the deeper layers would include relatively large uncertainty at present. In future work, we will improve the model for quantitative simulation of the spatiotemporal variation of fine particulate matter in both seawater and sediment. We will perform long-term simulations including the tsunami disturbance to validate the model, using recent observations of vertical sedimentary ^{137}Cs distribution.

Appendix A: Statistical method to evaluate model performance

The factor FA_n (e.g. Draxler, 2006) indicates the percentage of the population of the simulated results that satisfy

$$\frac{1}{n} \leq \frac{\text{Sim}}{\text{Obs}} \leq n, \quad (\text{A1})$$

where Obs and Sim are the observed and simulated results respectively.

FB (e.g. Draxler, 2006) is the normalized difference between the average of the observations and that of the simulations, as defined by

$$\text{FB} = \frac{\overline{\text{Sim}} - \overline{\text{Obs}}}{(\overline{\text{Sim}} + \overline{\text{Obs}}) / 2}, \quad (\text{A2})$$

where $\overline{\text{Obs}}$ and $\overline{\text{Sim}}$ are the averages of Obs and Sim respectively. The FB value ranges from -2 to 2 , and a positive/negative value indicates overestimation/underestimation.

The Supplement related to this article is available online at doi:10.5194/bg-12-7107-2015-supplement.

Acknowledgements. We acknowledge MEXT and the Nuclear Regulation Authority for providing the observation datasets. We also thank the Japan Agency for Marine-Earth Science and Technology for providing the FRA-JCOPE data set. Special thanks go to Akio Imai and Hiroshi Koshikawa for their insightful comments and encouragement. We are grateful for comments and suggestions from anonymous reviewers and the managing editors. The simulations were performed using supercomputer system NEC SX-9/A(ECO) of the National Institute for Environmental Studies.

Edited by: C. Woulds

References

- Ambe, D., Kaeriyama, H., Shigenobu, Y., Fujimoto, K., Ono, T., Sawada, H., Saito, H., Miki, S., Setou, T., Morita, T., and Watanabe, T.: Five-minute resolved spatial distribution of radionuclides in sea sediment derived from the Fukushima Daiichi Nuclear Power Plant, *J. Environ. Radioactiv.*, 138, 264–275, doi:10.1016/j.jenvrad.2014.09.007, 2014.
- Aoyagi, K. and Igarashi, S.: On the size distribution of sediments in the coastal sea of Fukushima Prefecture, *Bull. Fukushima Prefecture Fish. Exp. Station*, 8, 69–81, 1999 (in Japanese).
- Blaas, M., Dong, C., Marchesiello, P., McWilliams, J. C., and Stolzenbach, K. D.: Sediment-transport modeling on Southern Californian shelves: a ROMS case study, *Cont. Shelf Res.*, 27, 832–853, 2007.
- Buesseler, K., Aoyama, M., and Fukasawa, M.: Impacts of the Fukushima nuclear power plants on marine radioactivity, *Environ. Sci. Technol.*, 45, 9931–9935, doi:10.1021/es202816c, 2011.
- Buesseler, K. O., Jayne, S. R., Fisher, N. S., Rypina, I. I., Baumann, H., Baumann, Z., Breier, C. F., Douglass, E. M., George, J., Macdonald, A. M., Miyamoto, H., Nishikawa, J., Pike, S. M., and Yoshida, S.: Fukushima-derived radionuclides in the ocean and biota off Japan, *P. Natl. Acad. Sci. USA*, 109, 5984–5988, 2012.
- Chino, M., Nakayama, H., Nagai, H., Terada, H., Katata, G., and Yamazawa, H.: Preliminary estimation of release amounts of ¹³¹I and ¹³⁷Cs accidentally discharged from the Fukushima daiichi nuclear power plant into the atmosphere, *J. Nucl. Sci. Technol.*, 48, 1129–1134, 2011.
- Choi, Y., Kida, S., and Takahashi, K.: The impact of oceanic circulation and phase transfer on the dispersion of radionuclides released from the Fukushima Dai-ichi Nuclear Power Plant, *Biogeosciences*, 10, 4911–4925, doi:10.5194/bg-10-4911-2013, 2013.
- Deltares: Delft3D-FLOW User Manual, Simulation of Multi-Dimensional Hydrodynamic Flows and Transport Phenomena, Including Sediments, Version: 3.15.25157, Deltares, the Netherlands, 674 pp., 2012.
- Draxler, R. R.: The Use of global and mesoscale meteorological model data to predict the transport and dispersion of tracer plumes over Washington, D.C., *Weather Forecast.*, 21, 383–394, doi:10.1175/WAF926.1, 2006.
- Draxler, R., Arnold, D., Galmarini, S., Hort, M., Jones, A., Leadbetter, S., Malo, A., Maurer, C., Rolph, G., Saito, K., Servranckx, R., Shimbori, T., Solazzo, E., and Wotawa, G.: Evaluation of Meteorological Analyses For the Radionuclide Dispersion and Deposition From the Fukushima Daiichi Nuclear Power Plant Accident, WMO-No. 1120, World Meteorological Organization, Switzerland, 64 pp., available at: http://library.wmo.int/opac/index.php?lvl=notice_display&id=15838 (last access: 8 June 2015), 2013.
- Flather, R. A.: A tidal model of the northwest European continental shelf, *Memories de la Societe Royale des Sciences de Liege*, 6, 141–164, 1976.
- Fossing, H., Berg, P., Thamdrup, B., Rysgaard, S., Sørensen, H. M., and Nielsen, K.: A Model Set-Up For an Oxygen and Nutrient Flux Model For Aarhus Bay (Denmark), NERI Technical Report No. 483, National Environmental Research Institute, Denmark, 65 pp., 2004.
- Furuichi, N. and Hibiya, T.: Assessment of the upper-ocean mixed layer parameterizations using a large eddy simulation model, *J. Geophys. Res.*, 120, 2350–2369, doi:10.1002/2014JC010665, 2015.
- Furuichi, N., Hibiya, T., and Niwa, Y.: Assessment of turbulence closure models for resonant inertial response in the oceanic mixed layer using a large eddy simulation model, *J. Oceanogr.*, 68, 285–294, doi:10.1007/s10872-011-0095-3, 2012.
- Higashi, H., Koshikawa, H., Murakami, S., and Kohata, K.: A long-term simulation study on variability of short-necked clam resources in Ise Bay in the 1990s, *Journal of Japan Society of Civil Engineers, Ser. B2 (Coastal Engineering)*, 67, I_1046–I_1050, doi:10.2208/kaigan.67.I_1046, 2011 (in Japanese with English abstract).
- Higashi, H., Furuichi, N., and Maki, H.: Validation of Vertical Mixing Schemes Based on In-situ Turbulence Measurements in Tokyo Bay, *J. Jpn Soc. Civil Engineers, Ser. B2 (Coastal Engineering)*, 69, I_1066–I_1070, doi:10.2208/kaigan.69.I_1066, 2013 (in Japanese with English abstract).
- Higashi, H., Morino Y., and Ohara, T.: A numerical study on oceanic dispersion and sedimentation of radioactive Cesium-137 from Fukushima Daiichi nuclear power plant, *Journal of Japan Society of Civil Engineers, Ser. B2 (Coastal Engineering)*, 70, I_1121–I_1125, doi:10.2208/kaigan.70.I_1121, 2014 (in Japanese with English abstract).
- Hirt, C. W. and Nichols, B. D.: Volume of fluid method for the dynamics of free boundaries, *J. Comput. Phys.*, 39, 201–225, 1981.
- Kawamura, H., Kobayashi, T., Furuno, A., In, T., Ishikawa, Y., Nakayama, T., Shima, S., and Awaji, T.: Preliminary numerical experiments on oceanic dispersion of ¹³¹I and ¹³⁷Cs discharged into the ocean because of the Fukushima daiichi nuclear power plant disaster, *J. Nucl. Sci. Technol.*, 48, 1349–1356, 2011.
- Kobayashi, T., Otosaka, S., Togawa, O., and Hayashi, K.: Development of a non-conservative radionuclides dispersion model in the ocean and its application to surface cesium-137 dispersion in the Irish Sea, *J. Nucl. Sci. Technol.*, 44, 238–247, doi:10.1080/18811248.2007.9711278, 2007.
- Kobayashi, T., Nagai, H., Chino, M., and Kawamura, H.: Source term estimation of atmospheric release due to the Fukushima Daiichi Nuclear Power Plant accident by atmospheric and

- oceanic dispersion simulations, *J. Nucl. Sci. Technol.*, 50, 255–264, doi:10.1080/00223131.2013.772449, 2013.
- Kondo, J.: Air-sea bulk transfer coefficients in diabatic conditions, *Bound.-Lay. Meteorol.*, 9, 91–112, 1975.
- Kusakabe, M., Oikawa, S., Takata, H., and Misonoo, J.: Spatiotemporal distributions of Fukushima-derived radionuclides in nearby marine surface sediments, *Biogeosciences*, 10, 5019–5030, doi:10.5194/bg-10-5019-2013, 2013.
- Lesser, G. R., Roelvink, J. A., van Kester, J. A. T. M., and Stelling, G. S.: Development and validation of a three-dimensional morphological model, *Coast. Eng.*, 51, 883–915, 2004.
- Matsumoto, K., Takanezawa, T., and Ooe, M.: Ocean tide models developed by assimilating TOPEX/POSEIDON altimeter data into hydrodynamical model: a global model and a regional model around Japan, *J. Oceanogr.*, 56, 567–581, 2000.
- Masumoto, Y., Miyazawa, Y., Tsumune, D., Kobayashi, T., Estournel, C., Marsaleix, P., Lanerolle, L., Mehra, A., and Garrao, Z. D.: Oceanic dispersion simulation of Cesium 137 from Fukushima Daiichi Nuclear Power Plant, *Elements*, 8, 207–212, 2012.
- MEXT (Ministry of Education, Culture, Sports, Science and Technology): Monitoring Information of Environmental Radioactivity Level, available at: <http://radioactivity.nsr.go.jp/en/> (last access: 8 June 2015), 2011.
- MOE (Ministry of Environment): Radioactive Material Monitoring Surveys of the Water Environment, available at: <http://www.env.go.jp/en/water/rmms/surveys.html> (last access: 8 June 2015), 2011.
- Misumi, K., Tsumune, D., Tsubono, T., Tateda, Y., Aoyama, M., Kobayashi, T., and Hirose, K.: Factors controlling the spatiotemporal variation of ¹³⁷Cs in seabed sediment off the Fukushima coast: implications from numerical simulations, *J. Environ. Radioactiv.*, 136, 218–228, doi:10.1016/j.jenvrad.2014.06.004, 2014.
- Miyazawa, Y., Zhang, R., Guo, X., Tamura, H., Ambe, D., Lee, J. S., Okuno, A., Yoshinari, H., Setou, T., and Komatsu, K.: Water mass variability in the western North Pacific detected in a 15-year eddy resolving ocean reanalysis, *J. Oceanogr.*, 65, 737–756, 2009.
- Miyazawa, Y., Masumoto, Y., Varlamov, S. M., and Miyama, T.: Transport simulation of the radionuclide from the shelf to open ocean around Fukushima, *Cont. Shelf Res.*, 50–51, 16–29, doi:10.1016/j.csr.2012.09.002, 2012.
- Miyazawa, Y., Masumoto, Y., Varlamov, S. M., Miyama, T., Takigawa, M., Honda, M., and Saino, T.: Inverse estimation of source parameters of oceanic radioactivity dispersion models associated with the Fukushima accident, *Biogeosciences*, 10, 2349–2363, doi:10.5194/bg-10-2349-2013, 2013.
- Monte, L., Periañez, R., Boyer, P., Smith, J. T., and Brittain, J. E.: The role of physical processes controlling the behaviour of radionuclide contaminants in the aquatic environment: a review of state-of-the-art modelling approaches, *J. Environ. Radioactiv.*, 100, 779–784, doi:10.1016/j.jenvrad.2008.05.006, 2009.
- Morino, Y., Ohara, T., and Nishizawa, M.: Atmospheric behavior, deposition, and budget of radioactive materials from the Fukushima Daiichi nuclear power plant in March 2011, *Geophys. Res. Lett.*, 38, L00G11, doi:10.1029/2011GL048689, 2011.
- Murakami, K., Suganuma, F., and Sasaki, H.: Experimental Investigation on Erosion and Deposition of Fine Cohesive Sediments in an Annular Rotating Channel, Report of the Port and Harbour Research Institute, 28, Japan, 43–76, 1989.
- Nakanishi, M. and Niino, H.: Development of an improved turbulence closure model for the atmospheric boundary layer, *J. Meteorol. Soc. Jpn.*, 87, 895–912, 2009.
- NRA (Nuclear Regulation Authority): Achievement Report on Measurement and Study of Radionuclide Distribution in Ocean in 2013 Japanese Fiscal Year, available at: http://radioactivity.nsr.go.jp/ja/contents/10000/9423/24/report_20140613.pdf (last access: 8 June 2015), 2014a (in Japanese).
- Nuclear Regulation Authority (NRA): Monitoring Information of Environmental Radioactivity Level, available at: <http://radioactivity.nsr.go.jp/en/> (last access: 8 June 2015), 2014b.
- Otosaka, S. and Kato, Y.: Radiocesium derived from the Fukushima Daiichi Nuclear Power Plant accident in seabed sediments: initial deposition and inventories, *Environ. Sci.: Proc. Impacts*, 16, 978–990, doi:10.1039/c4em00016a, 2014.
- Otosaka, S. and Kobayashi, T.: Sedimentation and remobilization of radiocesium in the coastal area of Ibaraki, 70 km south of the Fukushima Dai-ichi Nuclear Power Plant, *Environ. Monit. Assess.*, 185, 5419–5433, doi:10.1007/s10661-012-2956-7, 2013.
- Periañez, R.: Redissolution and long-term transport of radionuclides released from a contaminated sediment: a numerical modelling study, *Estuar. Coast. Shelf S.*, 56, 5–14, 2003a.
- Periañez, R.: Kinetic modelling of the dispersion of plutonium in the eastern Irish Sea: two approaches, *J. Marine Syst.*, 38, 259–275, 2003b.
- Periañez, R.: Testing the behaviour of different kinetic models for uptake-release of radionuclides between water and sediments when implemented on a marine dispersion model, *J. Environ. Radioactiv.*, 71, 243–259, 2004.
- Periañez, R.: A modelling study on ¹³⁷Cs and ^{239,240}Pu behaviour in the Alborán Sea, western Mediterranean, *J. Environ. Radioactiv.*, 99, 694–715, 2008.
- Periañez, R., Suh, K. S., and Min, B. I.: Local scale marine modelling of Fukushima releases, Assessment of water and sediment contamination and sensitivity to water circulation description, *Mar. Pollut. Bull.*, 64, 2333–2339, doi:10.1016/j.marpolbul.2012.08.030, 2012.
- Reed, C. W., Niedoroda, A. W., and Swift, D. J. P.: Modeling sediment entrainment and transport processes limited by bed armoring, *Mar. Geol.*, 154, 143–154, 1999.
- Smagorinsky, J.: General circulation experiments with the primitive equations, I. The basic experiment, *Mon. Weather Rev.*, 91, 99–164, 1963.
- Sohma, A., Sekiguchi, Y., Kuwae, T., and Nakamura, Y.: A benthic-pelagic coupled ecosystem model to estimate the hypoxic estuary including tidal flat – model description and variation of seasonal/daily dynamics, *Ecol. Model.*, 215, 10–39, doi:10.1016/j.ecolmodel.2008.02.027, 2008.
- Sternberg, R. W., Berhane, I., and Ogston, A. S.: Measurement of size and settling velocity of suspended aggregates on the northern California continental shelf, *Mar. Geol.*, 154, 43–53, 1999.
- Stohl, A., Seibert, P., Wotawa, G., Arnold, D., Burkhardt, J. F., Eckhardt, S., Tapia, C., Vargas, A., and Yasunari, T. J.: Xenon-133 and caesium-137 releases into the atmosphere from the Fukushima Dai-ichi nuclear power plant: determination of the

- source term, atmospheric dispersion, and deposition, *Atmos. Chem. Phys.*, 12, 2313–2343, doi:10.5194/acp-12-2313-2012, 2012.
- Terada, H., Katata, G., Chino, M., and Nagai, H.: Atmospheric discharge and dispersion of radionuclides during the Fukushima Dai-ichi Nuclear Power Plant accident. Part II: verification of the source term and analysis of regional-scale atmospheric dispersion, *J. Environ. Radioactiv.*, 112, 141–154, 2012.
- TEPCO (Tokyo Electric Power Corporation): Influence to Surrounding Environment, Archives, available at: www.tepco.co.jp/en/nu/fukushima-np/f1/index2-e.html (last access: 8 June 2015), 2011.
- Thornton, B., Ohnishi, S., Ura, T., Odano, N., Sasaki, S., Fujita, T., Watanabe, T., Nakata, K., Ono, T., and Ambe, D.: Distribution of local ^{137}Cs anomalies on the seafloor near the Fukushima Dai-ichi Nuclear Power Plant, *Mar. Pollut. Bull.*, 74, 344–350, doi:10.1016/j.marpolbul.2013.06.031, 2013.
- Tsumune, D., Tsubono, T., Aoyama, M., and Hirose, K.: Distribution of oceanic ^{137}Cs from the Fukushima Dai-ichi Nuclear Power Plant simulated numerically by a regional ocean model, *J. Environ. Radioactiv.*, 111, 100–108, 2012.
- Tsumune, D., Tsubono, T., Aoyama, M., Uematsu, M., Misumi, K., Maeda, Y., Yoshida, Y., and Hayami, H.: One-year, regional-scale simulation of ^{137}Cs radioactivity in the ocean following the Fukushima Dai-ichi Nuclear Power Plant accident, *Biogeosciences*, 10, 5601–5617, doi:10.5194/bg-10-5601-2013, 2013.
- Ushijima, S., Takemura, M., and Nezu, I.: Investigation on computational schemes for MAC methods with collocated grid system, *J. Jpn Soc. Civil Engineers*, 719, 11–19, 2002 (in Japanese with English abstract).
- Yasuda, I., Okuda, K., and Shimizu, Y.: Distribution and modification of the North Pacific Intermediate Water in the Kuroshio-Oyashio Interfrontal zone, *J. Phys. Oceanogr.*, 26, 448–465, 1996.